TROPICAL NORTH ATLANTIC HYDROLOGIC CYCLE VARIABILITY IN THE FLORIDA STRAITS DURING THE LAST ICE AGE

A Thesis

by

THEODORE ROLAND THEM, II

Submitted to the Office of Graduate Studies of
Texas A&M University
in partial fulfillment of the requirements for the degree of

MASTER OF SCIENCE

August 2012

Major Subject: Oceanography

Tropical North Atlantic Hydrologic Cycle Variability in the Florida Straits During the Last Ice Age

TROPICAL NORTH ATLANTIC HYDROLOGIC CYCLE VARIABILITY IN THE FLORIDA STRAITS DURING THE LAST ICE AGE

A Thesis

by

THEODORE ROLAND THEM, II

Submitted to the Office of Graduate Studies of
Texas A&M University
in partial fulfillment of the requirements for the degree of

MASTER OF SCIENCE

Approved by:

Chair of Committee,	Matthew W. Schmidt
Committee Members,	Niall C. Slowey
	Franco Marcantonio
Head of Department,	Piers Chapman

August 2012

Major Subject: Oceanography

ABSTRACT

Tropical North Atlantic Hydrologic Cycle Variability in the Florida Straits During the Last Ice Age.

(August 2012)

Theodore Roland Them, II, B.S., Shippensburg University of Pennsylvania

Chair of Advisory Committee: Dr. Matthew W. Schmidt

Abrupt, millennial-scale climate oscillations, known as Dansgaard-Oeschger (D-O) cycles, characterized the climate system during the last ice age. Proxy evidence suggests these climate oscillations resulted in global-scale reorganizations in the hydrological cycle. For this study, Mg/Ca-paleothermometry and stable isotope measurements were combined on the planktonic foraminifera *Globigerinoides ruber* (white variety) from Florida Straits sediment core KNR166-2 JPC26 (24°19.61'N, 83°15.14'W; 546 m depth) to reconstruct a high-resolution record of sea surface temperature and $\delta^{18}O_{SW}$ (a proxy for upper water column salinity) during Marine Isotope Stages 2 and 3 from 20 – 35.45 ka BP. As additional proxies for upper water column salinity change, Ba/Ca ratios in *G. ruber* were also measured to determine the relative contribution of local riverine input on the $\delta^{18}O_{SW}$ record and a faunal abundance count record of the planktonic foraminifera *N. dutertrei* abundance was developed. These results show that rapid upper water column salinity changes occurred across D-O events in the Florida Straits, coeval with climate change in the high-latitude North Atlantic.

Furthermore, the *G. ruber* Ba/Ca record suggests that riverine-derived meltwater from the Gulf of Mexico did not significantly impact surface salinity in the Florida current, calling into question the role of Mississippi River discharge on Atlantic Meridional Overturning Circulation (AMOC) during MIS 2 and 3. Instead, the most likely cause of MIS 2 and 3 salinity changes in the Florida Straits were variations in the strength and position of the Intertropical Convergence Zone. Finally, the timing of surface salinity change was compared with the benthic $\delta^{18}O_C$ record from the same core. A recent study showed that benthic $\delta^{18}O_C$ changes on the Florida Margin can be combined with contemporaneous records from the Bahamas Margin to reconstruct Florida Current transport related to AMOC variability. These results show that atmospheric circulation changes lead AMOC changes on the transition out of cold stadial events, suggesting the trigger for these abrupt climate events may reside in the tropics rather than in the high-latitude North Atlantic as previously thought.

DEDICATION

This thesis is dedicated to Ian.

ACKNOWLEDGMENTS

I would first like to thank my committee chair, Matthew Schmidt. You gave me the opportunity to perform exciting and important research at a highly regarded academic institution. I cannot thank you enough, for you have turned me into a master isotopist, a title of which only a few may boast. I enjoyed our time in Europe. I also want to thank you for letting me go on the cruise to Shatsky Rise in the Pacific Ocean. The last two years have gone by so quickly; I cannot believe my time here is almost over. It feels like I was just getting started.

I would also like to thank my committee members Niall Slowey and Franco Marcantonio. Niall, I appreciate the patience you have had with me and your support in my unwavering endeavors to find a PhD project. You are a great mentor and scientist and I am honored to call you my friend.

Franco, I thoroughly enjoyed your presence in Prague and at my poster session at the Goldschmidt Conference. I hope my thesis defense makes a little more sense than my poster presentation.

Adrian, you have been a great friend and roommate. I don't think I would have made it this far or at least stayed sane without you! I'm looking forward to the many good times ahead.

I would like to thank my sister, Alexis, for your encouragement and support of my academic goals. I would also like to thank you beforehand for letting me stay at

your new house in the Finger Lakes over the summer before I begin my PhD, more so because I plan on visiting wineries the whole time.

Thanks to my mother and father for their encouragement, patience, and love. Furthermore, thank you for pushing me to work hard and appreciate education.

Jennifer, I want to thank you for being a great labmate. Good luck with the rest of your academic career.

Finally, thanks also go to my friends and colleagues and the department faculty and staff for making my time at Texas A&M University a great experience. I also want to extend my gratitude to the National Science Foundation P2C2 and S-STEM grants, which provided support to run samples at Texas A&M University's R. Ken William's Radiogenic Isotope Lab and NOSAMS, and also covered multiple semesters of tuition, fees, stipend, and travel support.

Goodbye, Texas. I'm sure I'll see you again.

NOMENCLATURE

AMOC	Atlantic Meridional Overturning Circulation
BP	Before Present
CCD	Carbonate Compensation Depth
D-O	Dansgaard-Oeschger
EPICA	European Project for Ice Coring in Antarctica
GCM	General Circulation Model
H	Heinrich
IRD	Ice Rafted Debris
ITCZ	Intertropical Convergence Zone
IVF	Ice Volume Free
Ka	Kiloannum
LGM	Last Glacial Maximum
LIS	Laurentide Ice Sheet
MIS	Marine Isotope Stage[s]
NGRIP	North Greenland Ice Core Project
SSS	Sea Surface Salinity
SST	Sea Surface Temperature
TNA	Tropical North Atlantic

TABLE OF CONTENTS

Page

LIST OF FIGURES

1. INTRODUCTION

Today, heat and salt are transported from low to high latitudes in the North Atlantic, via the Gulf Stream. These saline upper waters rapidly cool as they encounter the much colder high-latitude air temperatures and eventually become dense enough to sink and form North Atlantic Deep Water (NADW). NADW then flows south along the bottom of the Atlantic and eventually becomes part of the Circumpolar Deepwater Current flowing around Antarctica. The resulting circulation, known as Atlantic Meridional Overturning Circulation (AMOC), maintains a modern global transfer of heat from the South Atlantic to the North Atlantic. Previous research showed several significant periods of climate change resulting from variations in the strength of AMOC [*Lynch-Stieglitz et al.*, 1999a; *McManus et al.*, 2004; *Piotrowski et al.*, 2005; *Lund et al.*, 2006; *Praetorius et al.*, 2008; *Lynch-Stieglitz et al.*, 2011]. For example, during the Last Glacial Maximum (LGM), a time when much of North America and northern Europe were covered in massive ice sheets, AMOC strength was probably much weaker [*Lynch-Stieglitz et al.*,1999a].

While the Holocene epoch is characterized by a relatively warm and stable climate with little change in sea level, the last glacial cycle, represented by Marine Isotope Stages (MIS) 2, 3, and 4 (74 – 11 ka BP) in the benthic oxygen isotope record [*Shackleton and Opdyke*, 1973; *Shackleton et al.*, 1983], was characterized by

---

This thesis follows the style of *Paleoceanography*.

millennial-scale saw-tooth patterned climate oscillations, known as Dansgaard-Oeschger cycles [*Dansgaard et al*., 1993]. These abrupt warming and gradual cooling events (warm interstadials and cold stadials, respectively) were first discovered by analyzing the oxygen isotopic composition of Greenland ice cores [*Dansgaard et al*., 1969; *Dansgaard et al*., 1993]. Recent evidence suggested that these abrupt changes influenced climate on a global scale [*e.g.*, *Peterson et al.*, 2000; *Wang et al.*, 2001; *Voelker et al*, 2002; *Piotrowski et al*., 2005; *Schmidt et al*., 2006; *EPICA Community Members*, 2006; *Peterson and Haug*, 2006; *Wang et al.*, 2007; *Wang et al.*, 2008; *Clement and Peterson*, 2008; *Kanner et al.*, 2012].

The strength of the AMOC, which carries warm, saline tropical waters to the North Atlantic and induces density-driven overturning, is thought to be responsible for abrupt climate change during the last glacial cycle [*e.g.*, *Broecker et al.*, 1990; *Alley and Clark*, 1999; *Boyle*, 2000; *Rahmstorf*, 2002]. Alternatively, other researchers believe changes in atmospheric circulation could be the driver of millennial-scale climate events during the last ice age [*Cane and Clement*, 1999; *Jackson*, 2000; *Seager et al*., 2002; *Wunsch*, 2006].

High-resolution paleoproxy evidence is needed to confirm whether ocean circulation changes or atmospheric circulation changes are the driver of millennial-scale variability during MIS 3 [*Clement and Peterson*, 2008]. There is evidence of inferred AMOC weakening or shutdowns from proxy records [*Lynch-Stieglitz et al*., 1999a; *McManus et al*., 2004; *Praetorius et al.*, 2008; *Lynch-Stieglitz et al*., 2011], but it remains unclear whether atmospheric or ocean circulation changes triggered the abrupt

climate events [*Clement and Peterson*, 2008]. A recent study has attempted to uncover the trigger of these abrupt climate events during the last deglacial. *Schimdt and Lynch-Stieglitz* [2011] showed that during the transition into the Younger Dryas (abrupt cooling), the timing of ocean and atmosphere circulation changes were nearly synchronous. However, their data suggest there was a lead in tropical atmospheric reorganizations before ocean circulation changes occurred during the transition out of the Younger Dryas (abrupt warming) [*Schmidt and Lynch-Stieglitz*, 2011].

To develop a high-resolution climate record of sea surface temperature (SST) and surface salinity (SSS) change in the subtropical western North Atlantic during MIS 3 and into the LGM from 35.45 – 20 ka BP, and to determine the lead/lag relationship between millennial-scale atmospheric and oceanic circulation changes during this period oxygen isotopes and Mg/Ca ratios were measured in the planktonic foraminifera *Globigerinoides ruber* (white variety) from Florida Straits sediment core KNR 166-2 JPC26.

In an effort to determine changes in the tropical Atlantic hydrologic cycle resulting from abrupt shifts in atmospheric circulation patterns, a record of $\delta^{18}O_{SEAWATER}$ ($\delta^{18}O_{SW}$, a proxy for sea surface salinity) was then calculated. Changes in tropical Atlantic evaporation/precipitation (E – P) ratios associated with tropical hydrologic cycle changes have the potential to cause significant changes in local surface salinity, and thus $\delta^{18}O_{SW}$ values [*Schmidt et al.*, 2004] . For comparison a foraminiferal abundance count of the species *Neogloboquadrina dutertrei* was also performed as an additional proxy for relative changes in upper water column salinity.

The timing of reconstructed tropical Atlantic salinity changes was then compared to a recently reconstructed record of geostrophic flow variability through the Florida Straits based on oxygen isotope values in benthic foraminifera from JPC26, thought to reflect AMOC changes during MIS 2 and 3 [*Lynch-Stieglitz et al.*, in prep]. The use of this multi-proxy approach from a single core allows the direct comparison of the timing of atmospheric and ocean circulation changes across the abrupt climate events of MIS 2 and 3, independent of age model uncertainty, as recently done in *Schmidt and Lynch-Stieglitz* [2011] across the last deglacial period.

2. BACKGROUND

2.1. Proxy Reconstructions of the Last Glacial Cycle

Dansgaard et al. [1969] were the first group to observe significant variations (> 3 ‰) in the oxygen isotopic composition of glacial-aged ice ($\delta^{18}O_{ICE}$) cores from Greenland. Dansgaard *et al.* [1993] retrieved more ice cores as part of the joint European Greenland Ice-core Project (GRIP). The GRIP analyses corroborated *Dansgaard et al.* [1969]'s initial findings that the observed $\delta^{18}O_{ICE}$ oscillations were most likely caused by atmospheric temperature anomalies [*Dansgaard et al.*, 1993; *Charles et al.*, 1994]. Initially, these abrupt warming and gradual cooling periods were interpreted to have been resonant features of the last glacial cycle [*Dansgaard et al*., 1969; *Dansgaard et al.*, 1993], but it is generally understood that they are stochastic.

In addition to the abrupt interstadial transitions of the last ice age records preserved in the Greenland ice cores, marine sediments also record intervals during the last glacial cycle associated with the presence of large, terrestrial grains far from where rivers and glaciers would not have had any depositional influence [*e.g.*, *Heinrich*, 1988; *Bond et al.*, 1992; *Hemming*, 2004]. These deposits were traced thousands of kilometers from their original source and are thought to have been carried by floating icebergs. Therefore, these deposits are called ice-rafted debris (IRD) [*Heinrich*, 1988; *Bond et al.*, 1992]. These so called Heinrich events (H-events) are thought to be times of extremely cold conditions in the North Atlantic occurring near the end of some stadials.

The repetition of H-events during the last glacial cycle suggests that some factor

led to the growth and decay of continental ice sheets, possibly as "binge/purge cycles". A colder Northern Hemisphere would have aided the development and growth of ice sheets, such as North America's Laurentide Ice Sheet (LIS), with enhanced ice growth due to increasing albedo (ice-albedo effect). Eventually, the sheer mass of the ice sheets would have resulted in the eventual collapse of large sections. *MacAyeal* [1993a] showed the requisite physics for ice sheet binge/purge cycles at calculated H-event periodicities and *MacAyeal* [1993b] applied these fundamentals to explain how the LIS behaved on overlying bedrock.

Several general circulation models (GCMs) show that forcing a significant amount of freshwater into the northern North Atlantic at sites where deep water forms will induce a near or complete shutdown of AMOC. When AMOC shuts down, NADW ceases to form and the northward heat transport from the tropics is greatly reduced. As a result, the tropical/subtropical hydrologic cycle is altered by a southward shift in the mean positions of the Intertropical Convergence Zone (ITCZ) and Hadley circulation [*Vellinga and Wood*, 2002; *Lohmann*, 2003; *Dahl et al*., 2005; *Zhang and Delworth*, 2005; *Stouffer et al*., 2006]. Cooling of the North Atlantic reduces the overlying atmosphere's capability to hold water, which is compensated for by an increase in precipitation in the South Atlantic due to the southward shift of the ITCZ.

The ITCZ is manifested as a low pressure zone where the northeast and southeast trade winds converge. The large amount of solar heating near the equator leads to convective processes that cause air to rise and leads to extremely high amounts of precipiation. Today, the ITCZ is located farthest north during the late summer months in

the northern hemisphere. It then migrates south during boreal winter. Because of its location in the western tropical Atlantic, the circum-Caribbean region is sensitive to seaonal precipitation shifts associated with the annual migration of the ITCZ. In the Northern Hemisphere, these locations receive large amounts of precipitation during the summer and are generally drier during the winter. A quasi-permanent displacement of the ITCZ would therefore have significant effects on the tropical hydrologic cycle.

The atmospheric shift of the ITCZ to the south in response to North Atlantic cooling associated with AMOC shutdown is shown in other GCMs to have eventually restarted deep water formation in the North Atlantic [*Lohmann and Lorenz*, 2000; *Lohmann*, 2003; *Stouffer et al*., 2006; *Krebs and Timmermann*, 2007a; b]. Reduced salt export from the subtropical/tropical regions via NADW would have led to increased salinities in the northern Atlantic basin. These surface waters would eventually become more dense and subduct in the previously stratified water column [*Broecker et al*., 1990]. This would restart AMOC and shift the climate back into an interstadial mode. Due to the increased salt export via NADW during an interstadial, the process would eventually lead to another AMOC failure and the cycle would repeat itself. A recent reconstruction of subtropical gyre paleosalinities across some of the MIS 3 interstadials suggests that this mechanism may have played an important role in millennial-scale climate change [*Schmidt et al.*, 2006].

Other GCMs emphasize the role of atmospheric circulation changes play on abrupt climate change. During the LGM, ice sheets on the North American and northwestern European continents were large enough (large geographic distribution and

high elevations) that they acted as orographic barriers, with their spatial variability affecting large-scale wind field changes over the North Atlantic [*Romanova* et al., 2006; *Wunsch*, 2006]. An analogue to the LIS is the Rocky Mountains, which today affect stationary waves over North America and the Iceland Low, which in turn drastically affects wintertime climate over North America and northwestern Europe [*Seager et al*., 2002].

During the last glacial period, small changes in the elevation of the LIS would have greatly affected stationary atmospheric wave patterns over North America, which in turn may have affected AMOC variability [*Jackson*, 2000]. Oscillations in stationary wave patterns forced by variable LIS elevations could therefore be responsible for the abrupt climate oscillations recorded in Greenland $\delta^{18}O_{ICE}$ as interstadials [*Wunsch*, 2006].

2.2. The Use of Foraminiferal $\delta^{18}O$ in Proxy Records

The oxygen isotopic composition of foraminiferal calcite ($\delta^{18}O_C$) is primarily a function of the temperature and oxygen isotopic composition of the seawater ($\delta^{18}O_{SW}$) in which an individual precipitates its test [*Urey*, 1947; *Epstein and Mayeda*, 1953]. Therefore, it is necessary to determine the contribution of each of these factors.

The $\delta^{18}O$ of seawater reflects both the mean $\delta^{18}O$ of seawater, which is a function of the amount of continental ice, E – P dynamics, and source of water. The amount of continental ice has a large effect on mean $\delta^{18}O_{SW}$ and therefore $\delta^{18}O_C$, which varies

between glacial and interglacial periods [*e.g.*, *Duplessy et al.*, 1970; Shackleton and Opdyke, 1973]. During glacial periods, the lighter H_2O^{16} isotopologue is preferentially removed from ocean basins during evaporation, and these 'light' water molecules eventually precipitate out over the continents, leaving ice sheets extremely depleted in H_2O^{18} and causing the global $\delta^{18}O_{SW}$ value to inrease by about 1.0 ‰. When continental ice sheets melt on the glacial termination events, the highly enriched H_2O^{16} water then mixes back into the world oceans.

E – P, and hence sea surface salinity, is largely a function of the amount of rainfall in the open ocean. The mechanism is similar to that of the continental ice volume effect on $\delta^{18}O_{SW}$. If local evaporation rates are high, the H_2O^{16} isotopologue is preferentially removed and transported elsewhere, leaving seawater enriched in H_2O^{18} relative to H_2O^{16}.

2.3. The Use of Combined Foraminiferal Mg/Ca – $\delta^{18}O_C$ to Estimate $\delta^{18}O_{SW}$

In modern oceans, there are regionally existent linear relationships between $\delta^{18}O_{SW}$ and SSS. Due to the preferential evaporation of H_2O^{16}, it is possible to estimate SSS if the regional relationship is known. Currently, the most accurate way of calculating past $\delta^{18}O_{SW}$ change is to measure Mg/Ca ratios and $\delta^{18}O_C$ in foraminifera from the same shell material or same interval [*Mashiotta et al.*, 1999; *Lea et al.*, 2000; *Rosenthal et al.*, 2000; *Schmidt et al.*, 2004; *Schmidt et al.*, 2006]. The major assumption of using this method is that the $\delta^{18}O_{SW}$ – SSS relationship has not changed in

the past.

Previous studies showed that the low light *Orbulina universa* SST:$\delta^{18}O$ relationship [*Bemis et al.*,1998] properly estimates $\delta^{18}O_{SW}$ from *G. ruber* Mg/Ca-SST and $\delta^{18}O_C$ estimates [*Lea et al.*, 2000; *Schmidt et al.*, 2004; *Schmidt et al.*, 2006; *Schmidt and Lynch-Stieglitz*, 2011]. Therefore, the preferred method of reconstructing $\delta^{18}O_{SW}$ from *G. ruber* is by using the *Orbulina universa* low light equation from *Bemis et al.* [1998]:

$$T(°C) = 16.5 – 4.8(\delta^{18}O_C - \delta^{18}O_{SW}) \qquad [1]$$

In order to calculate $\delta^{18}O_{SW}$, it is necessary to independently determine temperature. Because the ratio of Mg/Ca in foraminiferal calcite is a function of temperature during shell calcification [*Nürnberg et al.*, 1996; *Mashiotta et al.*, 1999; *Lea et al.*, 1999; *Dekens et al.*, 2002; *Anand et al.*, 2003], this is possible. SSTs are reconsturcted from foraminiferal Mg/Ca ratios using the following Sargasso Sea sediment trap-based equation [*Anand et al.*, 2003]:

$$Mg/Ca = 0.38 \exp 0.09(SST) \qquad [2]$$

Paleosalinity reconstructions using these approaches have been very successful in determining the relative SSS changes across glacial-interglacial cycles [*Mashiotta et al.*, 1999; *Lea et al.*, 2000; *Schmidt et al.*, 2004] and millennial-scale oscillations [*Schmidt et al.*, 2006]. Other researchers have used this approach to look much further back in time to reconstruct continental ice volume changes through the Cenozoic and Mesozoic [*Lear et al.*, 2000; *Cramer et al.*, 2011].

Therefore, geographically broad reconstructions of glacial oceans should be

saltier than modern. This would result because of the vast amounts of freshwater stored in continental ice sheets such as the LIS. Within MIS 2 and 3, millennial-scale salinity oscillations can also be resolved if sedimentation rates are high enough.

2.4. The Use of Foraminiferal Mg/Ca Ratios to Estimate Calcification Temperature

The use of Mg/Ca paleothermometry reconstructions wasn't fully appreciated until the late 1990s [*Nürnberg et al.*, 1996a; *Hastings et al.*, 1998; *Mashiotta et al.*, 1999; *Elderfield and Ganssen*, 2000]. Because magnesium is a conservative element with a residence time in the oceans of 13 million years (Ma) [*Broecker and Peng*, 1982], late Quaternary paleotemperature reconstructions using Mg/Ca ratios in foraminiferal calcite are extremely useful tools for examining corresponding glacial and interglacial temperature changes [*Hastings et al.*, 1998; *Nürnberg et al.*, 2000; *Lea et al.*, 2000; *Barker et al.*, 2005].

Initial core top and culturing studies showed that the ratio of Mg/Ca in foraminiferal calcite increases exponentially by approximately 8 – 10 % per °C increase [*Nürnberg et al.*, 1996; *Mashiotta et al.*, 1999; *Lea et al.*, 1999]. Other studies showed that planktonic foraminifera living in the mixed layer faithfully record either mean annual sea surface temperatures (SSTs) or seasonal cycle variations [*Dekens et al.*, 2002; *Anand et al.*, 2003; *Schmidt et al.*, 2006], depending on geographic location.

Although Mg/Ca ratios incorporated during shell calcification in foraminifera

appear to be primarilly controlled by temperature [*e.g.*, *Nürnberg et al.*, 1996; *Mashiotta et al.*, 1999; *Lea et al.*, 1999; *Dekens et al.*, 2002; *Anand et al.*, 2003; *Ferguson et al.*, 2008; *Kisakürek et al.*, 2008; *Dueñas-Bohórquez et al.*, 2009], changes of pH and salinity are also a factor [*Nürnberg*, 1996; *Hastings et al.*, 1998; *Mashiotta et al.*, 1999; *Lea et al.*, 1999; *Kisakürek et al.*, 2008; *Dueñas-Bohórquez et al.*, 2009; *Mathien-Blard and Bassinot*, 2009; *Arbuszewski et al.*, 2010]. *Nürnberg et al.* [1996] showed that a 10 ‰ salinity change equated to a change in Mg of 110 % and suggested that large salinity increases result in increased metabolic activity. Other culturing studies show that small changes in salinity only have a minimal effect on shell Mg/Ca ratios [*Mashiotta et al.*, 1999; *Lea et al.*, 1999].

However, *Arbuszewski et al.* [2010] argue that Mg/Ca ratios increase by 27 % for each practical salinity unit (psu) increase above 35 in the planktonic foraminifer *Globigerinoides ruber* by analyzing a transect of deep-sea Atlantic Ocean core tops. These results are more dramatic than another study that evaluated core tops and plankton tows and found a salinity effect of 15% on Mg/Ca ratios in *Globigerinoides ruber* [*Mathien-Blard and Bassinot*, 2009]. It seems that a disparity exists between results of culturing vs. plankton tow and core top studies. Culturing studies tend to suggest that there is a small but statistically significant salinity effect on Mg/Ca ratios (~5 ± 3%) [*Nürnberg et al.*, 1996a; *Mashiotta et al.*, 1999; *Lea et al.*, 1999; *Kisakürek et al.*, 2008; *Dueñas-Bohórquez et al.*, 2009], whereas plankton tow and core top studies suggest an enhanced salinity effect [*Mathien-Blard and Bassinot*, 2009; *Arbuszewski et al.*, 2010].

In a recent study also based on core JPC26, *Schmidt and Lynch-Stieglitz* [2011]

showed that the use of the multivariate SST and SSS equations from *Arbuszewski et al.* [2010] resulted in unrealistic temperatures across the last deglacial. Therefore, this study uses the sediment trap Mg/Ca:SST relationship from *Anand et al.* [2003] to calculate past temperature change in the Florida Straits.

2.5. The Use of Foraminiferal Ba/Ca Ratios as an Indicator of Riverine Input

The use of Ba/Ca ratios in fossil foraminifera as a meltwater proxy is a relavtively novel approach. The majority of barium enters the ocean through riverine input [*Martin and Meybeck*, 1979] and through hydrothermal vent processes [*Edmond et al.*, 1979; *Von Damm et al.*, 1985]. In freshwater environments (*e.g.*, lakes and rivers) Ba^{2+} is desorbed from suspended sediments and results in riverine Ba^{2+} concentrations ($[Ba^{2+}]$) that are much higher than surface marine waters. When riverine water enters higher salinity estuaries the suspended sediment fine fraction flocculates and sinks. This results in brackish waters with high $[Ba^{2+}]$. As these waters mix with the much more saline marine waters, a conservative mixing line results, and an inverse relationship between $[Ba^{2+}]$ and salinity is observed [*Hanor and Chan*, 1977; *Edmond et al.*, 1978; *Coffey et al.*, 1997]. Laboratory experiments have shown that the incorporation of Ba^{2+} into living planktonic foraminifera is primarily a function of seawater $[Ba^{2+}]$ [*Lea and Spero*, 1994; *Hönisch et al.*, 2011]. Therefore, Ba/Ca ratios in foraminifera from a continental margin site can potentially be used as an indicator of riverine input [*Hall and Chan*, 2004; *Weldeab et al.*, 2007; *Schmidt and Lynch-Stieglitz*, 2011].

The use of foraminiferal Ba/Ca ratios is explored as an indicator of riverine input into the Gulf of Mexico during MIS 2 and 3. Because riverine water is enriched in ^{16}O relative to ^{18}O, it may be possible to determine periods when the salinity record ($\delta^{18}O_{IVF\text{-}SW}$) is affected by meltwater discharge during MIS 2 and 3.

2.6. The Use of *Neogloboquadrina dutertrei* as an Indicator of Relative Salinity

Another potential indicator of relative salinity is the fossil faunal abundance of the planktonic foraminifer *Neogloboquadrina dutertrei*. This species of foraminifera is a thermocline-dweller that is linked to eutrophic waters [*Fairbanks et al.*, 1982; *Schmuker and Schiebel*, 2002; *Rasmussen and Thomsen*, 2012] and has been used as an indicator of past low salinity (freshening) events in several ocean basins [*Ruddiman*, 1971; *Cullen*, 1981; *Kennett et al.*, 1985; *Maslin and Burns*, 2000; *Rasmussen and Thomsen*, 2012].

The *N. dutertrei* abundance record from JPC26 is therefore a useful tool to assess the veracity of both the reconstructed salinity ($\delta^{18}O_{IVF\text{-}SW}$) and riverine input (Ba/Ca) records. Periods of low salinity related to E – P dynamics and/or relative increases in riverine input to the Florida Straits should correlate to periods of increased abundance of *N. dutertrei*.

2.7. Potential Diagenetic Effects on Foraminiferal Calcite

Shell dissolution is linked to lower Mg/Ca ratios and more enriched $\delta^{18}O$ values in foraminifera [*Farrell and Prell*, 1989; *McCorkle et al.*, 1995; *Brown and Elderfield*, 1996; *Rosenthal et al.*, 2000].

Because pressure and therefore water depth directly affect the solubility of calcium carbonate, there is a zone of the ocean where the amount of carbonate dissolution increases with depth. The depth range where this reaction is active is called the lysocline. Below the lysocline is an area where the amount of calcium carbonate being created is in equilibrium with the amount being dissolved and is called the carbonate compensation depth (CCD) [*Berger*, 1968]. Below the CCD the influx of calcium carbonate that is deposited on the ocean floor should be near zero.

Therefore, studies that utilize the chemical composition of carbonate-based organisms extracted from deep sea sediments must identify if samples are affected by diagenetic processes. Studies must also take into account if shifting of the lysocline and CCD in the past had any effect on calcite preservation, which is different in each ocean basin [*Farrell and Prell*, 1989]. The combination of calcium carbonate fluxes, bottom water chemistry, and redox conditions due to organic carbon remineralization have an effect on this calcite saturation horizon, and therefore shell chemistry [*Brown and Elderfield*, 1996]. Because core JPC26 was recovered from a depth of only 546 m, it is located well above the Atlantic lysocline and CCD. Therefore, dissolution of our samples is not an issue. Furthermore, the presence of spines attached to *G. ruber* and the

presence of diagenetically susceptible pteropods throughout the core adds credence to dissolution having no effect on JPC26 samples.

3. OCEANOGRAPHIC SETTING

Core KNR166-2 JPC26 (24°19.61'N, 83°15.14'W; 546 m depth) is located in the Florida Straits near the Dry Tortugas (Figure 1). The Florida Current is comprised of wind-driven recirculated gyre water (~17 Sv) and cross-equatorial flow from the South Atlantic (~13 Sv) [*Schmitz & McCartney*, 1993]. These surface waters compensate the southward flow of NADW and represent the northward flowing surface branch of AMOC. The waters above this site originate from Caribbean, the tropical Atlantic and western tropical South Atlantic regions and reach the Florida Straits by flowing through the Yucatan Current [*Murphy et al.*, 1991; *Schmitz and Richardson*, 1991]. Thus, these waters maintain physical and chemical properties that are generally characteristic of the Caribbean, with the small potential to be influenced by currents originating in the Gulf of Mexico.

The modern average annual SST in the Florida Straits is 27.5°C, with a seasonal cycle that varies from a minimum of 25.0 to 26.0°C from December to March and a maximum of 29.0 – 29.4°C from July to September [*Locarnini et al.*, 2006]. Modern annual SSS off shore of the Dry Tortugas averages ~36.1, varying from a high of 36.1 to 36.2 from January to June and decreasing to a low of 35.9 from August to December [*Antonov et al.*, 2010].

Eddies are observed to form along the boundary of the Gulf of Mexico Loop Current near the Dry Tortugas and remain effectively stationary for days to months before finally dissipating [*Fratantoni et al.*, 1998]. These eddies result in SSTs that can

be cooler (>3°C) on the Florida Platform [*Fratantoni et al.*, 1998], but have no influence on the Bahamas margin of the Florida Straits. Because these phenomena are generally ephemeral, the recontstructed JPC26 SST record should not be significantly influenced, although effects of cold-core eddies will be taken into consideration if their effects are observable in this SST reconstruction.

The Florida Straits are also characterized by carbonate-rich environs. The shallow depth of the core (546 m), coupled with sediments with extremely high amounts of carbonate, result in fossil foraminifera that should not have been diagenetically altered by CCD shifts and other bottom water chemistry changes over glacial-interglacial periods. *Dekens et al.* [2002] suggested that a depth correction be used for *G. ruber* Mg/Ca ratios in sediments deeper than 2.8 km in the equatorial Atlantic. However, *G. ruber* with any evidence of diagenetic alteration (*e.g.*, pyrite formations, discolorations, thin shells, etc.) were not used in this study.

4. MATERIALS AND METHODS

4.1. Sedimentological Properties

Sedimentological properties of core KNR166-2 JPC26 were measured on board the R/V Knorr. A Multi-Sensor Track (MST) device was used to collect gamma-ray porosity, magnetic suscepbility, p-wave velocity, and resistivity. Another sedimentological property, coarse fraction, was measured during sample processing at Georgia Tech and Texas A&M. The coarse fraction represents the amount of sediments present that are greater than 63 μm per interval. These properties help detect any large-scale sedimentological processes that could have affected the core site stratigraphy, such as slumping. For example, down-slope processes may result in significant variations in coarse fraction and/or density due to the addition of coarser upslope sediments.

Sediments near the top of the core have a calculated density of ~1.7 g/cm^3 and generally increase to ~1.9 g/cm^3 near the bottom. This increase in density downcore is expected and is the result of compaction and dewatering because of increasing overburden pressures. During the time period of this study, small (~0.07 g/cm^3) density perturbations are observed and do not appear to signify the presence of mass transport deposits (Figure 2a).

The coarse fraction values from this study period increase from a minimum of ~10 % at the core bottom (35.45 ka BP) to ~30 % at ~28.6 ka BP and stay relatively constant for the rest of record to the LGM. Large-scale changes in coarse fraction are due to sedimentation rate changes across the deglacial (Figure 2b). Similar to the

density record (Figure 2a), there are no major changes in coarse fraction from 784.25 – 1118.25 cm indicative of mass transport deposits (Figure 2b). Therefore, a robust stratigraphic control is maintained during the study interval.

4.2. Stable Isotope Analyses

The planktonic foraminifera *G. ruber* (white variety) was picked in JPC26 at 2 cm intervals spanning 784.25 – 1120.25 cm. In order to lessen the chance of size-dependent isotope fractionation differences [*Lea et al.*, 2000; *Spero et al.*, 2003], *G. ruber* was picked from only the 250 – 355 μm size fraction. Stable isotopic analyses ($\delta^{18}O$ and $\delta^{13}C$) of 10-12 individuals were performed at Georgia Tech in the laboratory of Jean Lynch-Stieglitz using a GV Instruments Isoprime mass spectrometer with Multiprep or a Finnigan MAT 253 mass spectrometer with Kiel Device. Samples were picked, sonicated in methanol for approximately 3-8 seconds, and dried prior to isotope analysis.

4.3. Minor and Trace Metal Analyses

The abundances of metals in the foraminiferal calcite, expressed as metal/Ca (Me/Ca) ratios, were measured on the same intervals and size fraction of *G. ruber* specimens used for the stable isotope analyses. Around 580 μg of *G. ruber* shell material/sample (~35 – 45 shells) were crushed, homogenized, split and then cleaned for

trace element analyses according to the procedures of *Lea and Martin* [1996] and *Mashiotta et al.* [1999] without the DTPA step. Samples underwent three rinses in ultra-pure water, then two rinses in methanol, followed by two rinses in ultra-pure water. Next, samples were bathed in a hot reducing solution (ammonium citrate, ammonium hydroxide, and hydrazine) for 30 minutes and then an oxidizing solution (hydrogen peroxide and sodium hydroxide) for 10 minutes, and then transferred into new acid-leached micro-centrifuge vials. They were finally leached with a dilute ultra-pure acid solution (0.001 N HNO_3) and stored for minor and trace element analyses. All clean work was conducted in laminar flow benches under trace metal clean conditions. Using isotope dilution, as outlined in *Lea and Martin* [1996] and *Lea et al.* [2000], the samples were dissolved and analyzed for Me/Ca ratios on a Thermo Scientific Element XR High Resolution Inductively Coupled Plasma Mass Spectrometer (HR-ICP-MS) at Texas A&M University's R. Ken Williams Radiogenic Isotope Geosciences Laboratory. Approximately 90% of samples were replicated at least once.

In addition to quantifying shell Mg/Ca ratios, data were also collected on the following elements: Na, Sr, Ba, U, Al, Fe, and Mn. Analyses with high Al/Ca indicate the presence of detrital clays that were not removed during the cleaning process. Elevated levels of Fe/Ca or Mn/Ca indicate the presence of diagenetic coatings that were not removed during the cleaning process. Analyses with high (>100 μmol/mol) Al/Ca, Fe/Ca or Mn/Ca ratios or with low percent recovery (<20%) are normally rejected. Low percent recovery values usually indicate loss of shell material during the cleaning process, most likely due to human error.

4.4. Calculating $\delta^{18}O_{SW}$

Trace metal measurements are used to independently calculate SST and $\delta^{18}O_{SW}$. $\delta^{18}O_{SW}$ is reconstructed by using the *Orbulina universa* low light equation [1] [Bemis *et al.*, 1998]. SST is reconstructed by using equation [2] [*Anand et al.*, 2003]. Based on the assumption that sea level during the Last Glacial Maximum was 120 meters lower than present and that LGM $\delta^{18}O_{SW}$ value was 1.05 ‰ heavier than modern [*Schrag et al.*, 2002], a sea level change of 1 meter corresponds to a global $\delta^{18}O_{SW}$ change of 0.00875 ‰. This relationship is used to remove the influence of continental ice volume variability on calculated $\delta^{18}O_{SW}$, resulting in ice volume free $\delta^{18}O_{SW}$ ($\delta^{18}O_{IVF\text{-}SW}$), using a splice of two high resolution sea level curves available for early MIS 2 and and late MIS 3 [*Yokoyama et al.*, 2000; *Waelbroeck et al.*, 2002]. The calculated $\delta^{18}O_{IVF\text{-}SW}$ record reflects regional salinity oscillations in the Florida Straits from 20 – 35.45 ka BP. Furthermore, this surface water record is compared to the benthic $\delta^{18}O_{IVF\text{-}C}$ record, a proxy for Florida Straits transport [*Lynch-Stieglitz et al.*, in prep] in order to determine the lead/lag relationship between atmospheric and ocean circulation changes.

4.5. *Neogloboquadrina dutertrei* Abundance

The planktonic foraminfera *N. dutertrei* was counted from the >150 μm size fraction. This size fraction was split several times until at least 300 foraminifera remained [*Fatela and Taborda*, 2002]. After counting, the total number of individuals

of *N. dutertrei* was computed by multiplying the number counted by the fraction that remained after splitting. For example, if an interval was split 5 times, 1/32 of the total population remained. If 10 *N. dutertrei* were counted, then 10 was multiplied by 32 to result in a total population of 320. The total population of *N. dutertrei* per interval was then divided by the dry mass of the sediment from the correpsonding interval, resulting in the number of *N. dutertrei* per gram of sediment per interval. *N. dutertrei* were only considered if at least 60 % of the whole shell remained and could be unequivocally identified.

4.6. Age Model Development

The age model for JPC26 is based on eight radiocarbon-dated intervals for the period from 20 to 35.45 ka. Radiocarbon analyses of single or mixed species of planktonic foraminifera (*G. ruber* and *G. sacculifer*) were conducted at the National Ocean Sciences Accelerator Mass Spectrometry Facility (NOSAMS) at the Woods Hole Oceanographic Institution [see *Lynch-Stieglitz et al.*, 2011 for all but two of the raw ^{14}C values (878.25 cm and 1104.28 cm)]. Prior to analyses, samples were sonicated for 3-8 seconds in methanol to remove any loose organic materials, clays, and/or other small carbonate grains. Raw ^{14}C dates were converted to calendar years BP (most probable calendar age) using CALIB 6.0 [M. *Stuiver et al.*, Calib calibration program, version 6.0, 2011] using the standard marine reservoir correction of 400 years [*Hughen et al.*, 2004] (Table 1). Initially, an age model was deveoped by assuming linear sedimentation rates

between the most probable calendar ages for each radiocarbon-dated interval.

Several studies suggested that tropical North Atlantic temperature and hydrologic changes are correlated with climate change as recorded in the Greenland ice core records [*Peterson et al.*, 2000; *Wang et al.*, 2001; *Schmidt and Lynch*-Stieglitz, 2011]. Based on the initial radiocarbon-based age model, the timing of $\delta^{18}O_C$ change in the Florida Straits was compared to both the Greenland and Antarctica ice core records. The NGRIP $\delta^{18}O_{ICE}$ and Byrd $\delta^{18}O_{ICE}$ records were interpolated to 20 year time spacings using the Arand software package [*Howell et al.*, 2006] so comparisons could be made with the JPC26 $\delta^{18}O_C$ record. Ice core $\delta^{18}O_{ICE}$ values from the same or nearest chronological period were then chosen to calculate correlation coefficients between the JPC26 $\delta^{18}O_C$ record and the ice core records. Comparison of the JPC26 $\delta^{18}O_C$ and the NGRIP $\delta^{18}O_{ICE}$ records resulted in a correlation coefficient of -0.11, while the comparison between the JPC26 $\delta^{18}O_C$ and Byrd $\delta^{18}O_{ICE}$ records resulted in a correlation coefficient of 0. The lack of any correlation between the JPC26 $\delta^{18}O_C$ and Byrd $\delta^{18}O_{ICE}$ suggests that changes in high latitude southern hemisphere climate had little or no impact on tropical North Atlantic climate change during MIS 2 and MIS 3.

Given the relatively large uncertainty on the calibrated radiocarbon ages in our record, transitions within the JPC26 *G. ruber* $\delta^{18}O_C$ record were fine-tuned to transitions in the NGRIP $\delta^{18}O_{ICE}$ record across interstadials 2 – 7. Negative or positive $\delta^{18}O_C$ excursions were tuned into NGRIP record (Figure 3a). It should be noted that this tuning exercise did not change the calibrated ^{14}C ages beyond the original 2 σ error of the ages (Figure 3b). This resulted in a revised correlation coefficient of -0.35 between

the NGRIP record and the JPC26 $\delta^{18}O_C$ record across the entire record, and a correlation coefficient of -0.46 across interstadial 5.

Based on the tuned age model, sedimentation rates in JPC26 range from 12.6 cm/ka to 75.0 cm/ka during the study period (Figure 4). From 35.45 ka BP to 34.8 ka BP, sedimentation rates are 24.5 cm/ka. From 34.8 ka BP to 32.6 ka BP, sedimentation rates are 13.6 cm/ka. From 32.6 ka BP to 31.80 ka BP, sedimentation rates are 75.0 cm/ka. From 31.80 ka BP to 30.85 ka BP, sedimentation rates are 65.3 cm/ka. From 30.85 ka BP to 24.90 ka BP, sedimentation rates are 12.4 cm/ka. From 24.90 ka BP to 23.37 ka BP, sedimentation rates are 19.7 cm/ka. From 23.37 ka BP to 20.0 ka BP (top interval of this study), sedimentation rates are 19.0 cm/ka (Figure 4).

5. ERROR ANALYSIS

Long-term analytical precision for the planktonic $\delta^{18}O_C$ measurements is better than 0.08 ‰ based on replicate analyses of NBS-19 or in-house standards. The long-term analytical reproducibility of a synthetic, matrix-matched Mg/Ca standard analyzed by HR-ICP-MS over the course of this study is ±0.48%. The pooled standard deviation of all replicate Mg/Ca analyses is ±2.6 % (1 SD, degrees of freedom = 191) based on 356 analyzed intervals and the average Mg/Ca ratio is 3.56 mmol/mol, which equates to an error of ±0.09 mmol/mol, or ±0.28°C using equation [2].

Error on the calculated $\delta^{18}O_{SW}$ values was estimated by propagating the 1σ analytical error on the $\delta^{18}O_C$ values and the pooled standard deviation value on the Mg/Ca replicates with the reported error on calibration equations [1] and [2], resulting in an error of ±0.23 ‰. Previous studies report similar error propagations for $\delta^{18}O_{SW}$ residuals based on $\delta^{18}O_C$ and Mg/Ca-SSTs in *G. ruber* [*Carlson et al.*, 2008; *Lea et al.*, 2000; *Schmidt et al.*, 2004, 2006a; *Lund and Curry*, 2006; *Weldeab et al.*, 2006; *Oppo et al.*, 2009; *Schmidt and Lynch-Stieglitz*, 2011; *Schmidt et al.*, in press].

The long-term analytical reproducibility of a synthetic, matrix-matched Ba/Ca standard analyzed by HR-ICP-MS over the course of this study is ±0.47 %. The pooled standard deviation of all replicate Ba/Ca analyses is ±7.1 % (1 SD, degrees of freedom = 190) based on 355 analyzed intervals. The average Ba/Ca ratio in this study is 0.88 μmol/mol so the average analytical error for the Ba/Ca measurements in the JPC26 record is ±0.06 μmol/mol. Previous studies report similar errors on Ba/Ca ratios in *G.*

ruber [*Weldeab et al.*, 2007; *Schmidt and Lynch-Stieglitz*, 2011; *Schmidt et al.*, in press].

6. RESULTS

6.1. *G. ruber* $\delta^{18}O_C$

The *G. ruber* $\delta^{18}O_C$ values show an overall increasing trend from 35.45 – 20 ka BP, punctuated by several millennial-scale oscillations (Figure 5a). Across most of the interstadials, $\delta^{18}O_C$ is more negative (related to warmer and/or fresher waters), whereas the stadials are associated with more positive $\delta^{18}O_C$ values (related to colder and/or saltier waters).

Although the $\delta^{18}O_C$ record before 33.5 ka is variable with no clear trends, a significant 0.6 ‰ increase in $\delta^{18}O_C$ occurs at the transition into the stadial between interstadials 5 and 6.

As sedimentation rates drastically increase during interstadial 5, a much clearer millennial-scale $\delta^{18}O_C$ oscillation is evident in the JPC26 record. At 32.55 ka BP, a rapid decrease of ~1 ‰ occurs within 110 years, reaching a minimum at 32.44 ka BP. The gradual increase in $\delta^{18}O_C$ through the rest of the interstadial is similar to the NGRIP $\delta^{18}O_{ICE}$ record. After a stadial-like $\delta^{18}O_C$ increase occurs at 31.91 ka BP, another interstadial-like decrease in $\delta^{18}O_C$ values occurs in the JPC26 $\delta^{18}O_C$ record at 31.8 ka BP. This interstadial-like return to lighter $\delta^{18}O_C$ in JPC26 is not observed in the NGRIP record (Figure 5f). *G. ruber* $\delta^{18}O_C$ values then gradually increase from 31.8 – 28.92 ka BP, just before the transition into interstadial 4. No $\delta^{18}O_C$ changes are observed across H3. Interstadials 3 and 4 are marked by one point decreases in $\delta^{18}O_C$ values. However, constraining these portions of the record is difficult due to decreased sedimentation rates

in this section of the core.

The stadial after interstadial 3 is also marked by variable $\delta^{18}O_C$ values, but trend to heavier values. The most positive $\delta^{18}O_C$ value (0.97 ‰) occurs at 24.39 ka BP, just before the transition into H2. H2 is then marked by a large ~0.85 ‰ $\delta^{18}O_C$ decrease centered at 23.88 ka BP.

6.2. *G. ruber* Mg/Ca and Reconstructed Sea Surface Temperatures

Schmidt and Lynch-Stieglitz [2011] previously measured Mg/Ca ratios in *G. ruber* from JPC26 and their results showed a calculated core top temperature of 27.6°C using equation [2]. This estimated SST is nearly identical to the modern average annual SST at the core site of 27.5°C in the Florida Straits [*Locarnini et al.*, 2006], well within the ±1°C calibration uncertainty of equation [2] [*Anand et al.*, 2003]. Within the portion of JPC26 that represents MIS 2, the LGM has an average SST of 23.7°C (20 – 22.3 ka BP), which suggests a temperature difference that is ~3.8°C cooler than modern SSTs in the Florida Straits. The average Mg/Ca – SST across the entire record from 20 – 35.45 ka BP is 24.8°C. The coolest SSTs occur from 22.32 – 20 ka BP. Across the portion of the JPC26 that represents MIS 3, the lowest SSTs are ~23.5°C and generally occur during stadials, whereas the maximum SSTs are ~26.5°C and generally occur during interstadial portions of the record with the highest resolution (interstadials 5 and 7) (Figure 5b).

The highest resolution portion of the record from 32.57 – 30.85 ka BP shows a

clear warming during interstadials 5. In contrast, interstadial 6 shows a slight cooling of 1°C and interstadial 3 shows no temperature change. Interstadials 6 and 3 occur during the lowest resolution sections of the core (with five data points across interstadial 6 and three across interstadial 3); it is possible these temperature changes are associated with regional atmospheric temperature shifts.

Based on the tuned JPC26 age model, the bottom of the core is likely located near the transition into interstadial 7 (35.45 ka BP). Reconstructed SSTs in this interstadial show a cooling on the transition into the next stadial of approximately 2.5°C (35.45 – 34.7 ka BP). Interstadial 6 (three data points) shows a ~1°C cooling with a ~2°C warming across the transition into its corresponding stadial. The transition into interstadial 5 is not abrupt, but a warming of ~2°C occurs. The transition out of the interstadial is characterized by a gradual cooling of ~2°C. Similar to the previous stadial, Mg/Ca – SSTs begin to increase by ~1.5°C over 1,200 years. The rest of MIS 3 is characterized by a gradual decrease in SST of approximately 1.5°C (30.5 – ~27 ka BP). H3 is characterized by a slight SST cooling on the order of ~1.5°C. Similar to H3, H2 is also characterized by a slight SST cooling on the order of ~1.5°C.

MIS 2 Mg/Ca – SSTs in JPC26 are characterized by an initial gradual cooling at 24.7 ka BP. Furthermore, a significant warming of ~4°C is recorded from 23.3 – 23.1 ka BP, corresponding to interstadial 2. After this event, an abrupt cooling of 2°C occurs from 22.4 – 22.3 ka BP where SSTs drop to LGM values of 23.7°C.

6.3. Calculated $\delta^{18}O_{SW}$ and $\delta^{18}O_{IVF\text{-}SW}$ Record

G. ruber Mg/Ca – SST values are combined with paired $\delta^{18}O_C$ measurements to calculate $\delta^{18}O_{SW}$ using equation [1] [*Bemis et al.*, 1998] (Figures 6a and 5c). Interstadial 7 is initially characterized by heavier $\delta^{18}O_{SW}$ values, with a negative excursion occurring at 34.9 ka BP. The transition out of the interstadial is pronounced, with a 0.7 ‰ increase in $\delta^{18}O_{SW}$ at 34.5 ka BP. A short, two point negative $\delta^{18}O_{SW}$ excursion occurs during the transition into interstadial 6 around 33.5 ka BP. Another pronounced $\delta^{18}O_{SW}$ increase of 0.9 ‰ occurs at the transition into the next Greenland stadial at 33.3 ka BP. These heavier $\delta^{18}O_{SW}$ values characterize the stadial until the transition into the interstadial 5. A large and abrupt ~1.1 ‰ negative $\delta^{18}O_{SW}$ excursion occurs at 32.5 ka BP. A gradual increase of $\delta^{18}O_{SW}$ values continues into the next stadial (sawtooth-like pattern); however, a short negative 0.5 ‰ $\delta^{18}O_{SW}$ decrease is centered at 31.8 ka BP. A one point decrease in $\delta^{18}O_{SW}$ of ~0.5 ‰ occurs at 28.8 ka BP, which is centered on interstadial 4. A decreasing trend of $\delta^{18}O_{SW}$ decrease characterizes the next short stadial. Interstadial 3 is also characterized by a short, ~0.4 ‰ $\delta^{18}O_{SW}$ decrease centered at 27.6 ka BP. A trend towards more positive values occurs from 25.7 – 24.8 ka BP. Also, a very small $\delta^{18}O_{SW}$ decrease is observed across H3, but overall, this time period is characterized by very positive $\delta^{18}O_{SW}$ values relative to the rest of the record.

A pronounced $\delta^{18}O_{SW}$ change occurs during H2. Initially, $\delta^{18}O_{SW}$ values are very positive before a three point, 203 year $\delta^{18}O_{SW}$ decrease of ~0.7‰ that occurs around 24.1 ka BP. The observed lighter $\delta^{18}O_{SW}$ values in the Florida Straits during H2 are then

quickly reversed by a return to heavier $\delta^{18}O_{SW}$ values. This large increase in $\delta^{18}O_{SW}$ of ~1 ‰ after H2 is driven by the observed increase in *G. ruber* Mg/Ca – SSTs.

Next, a correction was made to the $\delta^{18}O_{SW}$ record to account for global $\delta^{18}O_{SW}$ change due to continental ice volume variation between 20 – 35.45 ka BP [*Schrag et al.*, 1996; *Yokoyama et al.*, 2000; *Waelbroeck et al.*, 2002]. Subtraction of global $\delta^{18}O_{SW}$ change (Figure 6b) results in the ice volume corrected $\delta^{18}O_{SW}$, $\delta^{18}O_{IVF\text{-}SW}$ record (Figures 6c and 5d).

It is apparent that millennial-scale salinity oscillations occurred in the Florida Straits during MIS 3 portion of JPC26. Because the highest sedimentation rates occur over the interstadial 5 time period, it is possible to resolve this event with high confidence. In general, $\delta^{18}O_{IVF\text{-}SW}$ minima (freshening) occur during interstadials, while stadials are characterized by more positive $\delta^{18}O_{IVF\text{-}SW}$ values (saltier).

At the end of interstadial 7, $\delta^{18}O_{IVF\text{-}SW}$ values increase by 0.7 ‰ at 34.5 ka BP. A short, two point negative $\delta^{18}O_{IVF\text{-}SW}$ excursion occurs during the transition into interstadial 6 around 33.5 ka BP. Another pronounced $\delta^{18}O_{IVF\text{-}SW}$ increase of 0.8 ‰ occurs at the transition into the next Greenland stadial at 33.3 ka BP. These heavier $\delta^{18}O_{IVF\text{-}SW}$ (salty) values characterize the stadial until the transition into interstadial 5. A large and abrupt ~1.1 ‰ negative $\delta^{18}O_{IVF\text{-}SW}$ excursion (freshening) occurs at 32.5 ka BP. A gradual increase of $\delta^{18}O_{IVF\text{-}SW}$ values continues into the next stadial (sawtooth-like pattern). A one point decrease of ~0.5 ‰ $\delta^{18}O_{IVF\text{-}SW}$ occurs at 28.8 ka BP, which is centered on interstadial 4. Fresher conditions generally characterize the next short stadial. Interstadial 3 is also characterized by a short, ~0.4 ‰ $\delta^{18}O_{IVF\text{-}SW}$ decrease

centered at 27.6 ka BP. A trend toward more positive $\delta^{18}O_{IVF\text{-}SW}$ values occurs from 25.7 – 24.8 ka BP. A small decrease in calculated $\delta^{18}O_{IVF\text{-}SW}$ values occurs across H3; however, this beginning of H2 is characterized by very positive $\delta^{18}O_{IVF\text{-}SW}$ values, suggesting very salty conditions. In contrast, a pronounced decrease in $\delta^{18}O_{IVF\text{-}SW}$ occurs during H2. Initially, conditions are very salty before a three point, ~200 year $\delta^{18}O_{IVF\text{-}SW}$ decrease of ~0.7‰ that occurs around 24.1 ka BP. The observed freshening in the Florida Straits during H2 is then quickly reversed by a return to salty conditions. This large increase in $\delta^{18}O_{IVF\text{-}SW}$ of ~1 ‰ after H2 is driven by the observed increase in *G. ruber* Mg/Ca – SSTs.

Because $\delta^{18}O_{SW}$ covaries linearly with SSS [*Craig and Gordon*, 1965; *Charles and Fairbanks*, 1990], it is possible to estimate salinity changes using this reconstructed $\delta^{18}O_{IVF\text{-}SW}$ Florida Straits record. Most of the waters at the Florida Straits study site originate in the Caribbean and tropical Atlantic [*Schmitz and Richardson*, 1991], so it is possible to estimate past salinity using the same modern $\delta^{18}O_{SW}$ – SSS relationship for the open Caribbean [*Schmidt et al.*, 1999 database]:

$$\delta^{18}O_{SW} \text{ ‰} = 0.3 * SSS - 9.8 \qquad [3]$$

Using the modern day $\delta^{18}O_{SW}$ – SSS relationship from the open-ocean Caribbean, SSS may be calculated the JPC26 *G. ruber* $\delta^{18}O_{IVF\text{-}SW}$ values (*e.g.*, *Schmidt and Lynch-Stieglitz*, 2011). Modern annual sea surface salinity off shore of the Dry Tortugas averages ~36.1 [*Antonov et al.*, 2010] and modern calculated $\delta^{18}O_{SW}$ is 0.95‰ [*Schmidt and Lynch-Stieglitz*, 2011]. Based on equation [3], the calculated average SSS in the JPC26 record from the LGM (from 20 – 22.3 ka BP) is 37.1 and the average early

MIS 3 SSS from 35.45 – 24.2 ka BP is 37.7. The average SSS for interstadial 5 is 36.5, very close to modern values.

6.4. *G. ruber* Ba/Ca

The lowest Ba/Ca ratios in JPC26 occur near the bottom of the core (~0.7 μmol/mol) (Figure 7c). Ba/Ca ratios increase by ~0.1 μmol/mol on the transition into interstadial 5. Afterwards, stadial Ba/Ca ratios tend to be higher than interstadials ratios by ~0.2 μmol/mol. There is an abrupt increase in Ba/Ca ratios of ~0.15 μmol/mol at 30.5 ka BP, followed by decreasing ratios for the next 800 years (including across H3). Another abrupt increase of ~0.2 μmol/mol is centered at 28.4 ka BP, which occurs at the end of interstadial 4. This is followed by a substantial decrease of ~0.25 μmol/mol at 27.9 ka BP. A small 0.15 μmol/mol increase occurs during interstadial 3 with an even larger (~0.3 μmol/mol) increase during the next stadial. An overall increasing trend to high Ba/Ca ratios is observed from 27 – 22.3 ka BP.

There is no significant change in Ba/Ca ratios across H2. However, a substantial increase of ~0.3 μmol/mol occurs at 23.2 ka BP , corresponding to the transition into the interstadial 2. Ba/Ca ratios at the beginning of the LGM at 22.4 ka BP are ~1.1 μmol/mol and slowly decrease to ~0.9 μmol/mol towards the start of this record at 20 ka BP.

6.5. *Neogloboquadrina dutertrei*

The number of *N. dutertrei* per gram of sediment is used to qualitatively determine relative upper water column salinity or productivity in the JPC26 record basins [*Ruddiman*, 1971; *Cullen*, 1981; *Fairbanks et al.*, 1982; *Kennett et al.*, 1985; *Maslin and Burns*, 2000; *Schmuker and Schiebel*, 2002; *Rasmussen and Thomsen*, 2012]. Initial observations suggest that a larger number of *N. dutertrei* were present during interstadials than during stadials (Figure 5e). These *N. dutertrei* data match the NGRIP $\delta^{18}O_{ICE}$ extremely well, which gives more confidence to the JPC26 age model considering it was tuned using a different variable ($\delta^{18}O_C$).

During interstadial 7, the average number of *N. dutertrei* per gram was 26.5. There are two noticeable spikes, one during the middle of the interstadial and another during the very end, but interstadial levels are maintained throughout this period. A decrease in the amount of *N. dutertrei* occurs during the interstadial – stadial transition and continues to decrease throughout the rest of the stadial. The transition into interstadial 6 is extreme and a change from 14.4 *N. dutertrei* per gram to 42.3 *N. dutertrei* per gram is centered at 33.6 ka BP, which is directly in the middle of the interstadial. The transition into the next stadial is marked by a drastic decrease in *N. dutertrei*, in which *N. dutertrei* were absent in nearly half of the corresponding intervals.

The transition into interstadial 5 is again marked by a rapid increase in the number of *N. dutertrei* per gram of sediment. There is a prominent saw-tooth pattern of *N. dutertrei* during the transition into the next stadial. Unlike the preceding stadials, the

number of *N. dutertrei* per gram of sediment begins an interstadial-like rise at 31.8 ka BP and maintains these values until stadial-like conditions return at 31 ka BP. The rest of the stadial maintains a low population of *N. dutertrei*. Similar to the $\delta^{18}O_{IVF\text{-}SW}$ record, there are no changes in *N. dutertrei* population abundance during H3 (Figure 5e). The transition into interstadial 4 is marked by another increase of *N. dutertrei* and remains high until 28.4 ka BP, before dropping dramatically during the middle of the next stadial. There is a very small increase in *N. dutertrei* abundance during interstadial 3 although this time period is not very well constrained due to reduced sedimentation rate at this time. An increase in the abundance of *N. dutertrei* from ~5 per gram to ~18 per gram is centered at 26.5 ka BP and is short in duration. There is a large increase in *N. dutertrei* (~3 per gram to ~26 per gram) centered at 24 ka BP, which occurs during H2. The rest of MIS 2 and the LGM are characterized by a very small abundance of *N. dutertrei*, but continuously present population (Figure 5e).

7. DISCUSSION

7.1. LGM and MIS 3 Sea Surface Temperature Changes

The millennial-scale sea surface temperature oscillations in the new JPC26 record appear to correlate to high-latitude climate change as recorded in the Greenland ice core records (Figure 5, B and F) [*Dansgaard et al.*, 1993; *NGRIP members*, 2004]. In general, interstadials result in higher Mg/Ca ratios in *G. ruber* and therefore warmer SSTs, consistent with warming observed in Greenland ice cores. A comparison of the whole JPC26 Mg/Ca record to the NGRIP $\delta^{18}O_{ICE}$ record yields a correlation coefficient of 0.06. However, across the highly resolved interstadial 5 portion of the JPC26 record, the correlation coefficient is 0.30. Both Heinrich events 2 and 3 are associated with a cooling of ~1.5°C (H3 is centered at 30 ka BP and H2 is centered at 23.98 ka BP).

Changes in tropical Northern Hemisphere precession could also be an important influence on the JPC26 SST record over longer time scales. Precession in the northern tropics was at a maximum around interstadial 5 at 30.5 ka BP and gradually decreased into the LGM (Figure 8). This may explain a portion of the SST decrease associated with LGM, which is a period when continental ice sheets were at their greatest extent.

In addition, there are several millennial-scale SST oscillations in the JPC26 record. The transition into interstadial 5 (32.47 – 32.23 ka BP) is marked by a large SST increase (~2°C). During the early part of this interstadial, *G. ruber* Mg/Ca – SSTs peak to near modern values, suggesting an abrupt return to near interglacial conditions (Figure 5b). A rapid resumption of AMOC during interstadials, as suggested by *Boyle* [2000]

and *Rasmussen and Thomsen* [2004], may have increased Florida Current transport and increased northward transport of heat out of the tropical Atlantic.

Hill et al. [2006] used Mg/Ca ratios in *G. ruber* (pink variety) to reconstruct sea surface temperatures in the Orca Basin (northern Gulf of Mexico) (Figure 1) from 28 – 45 ka BP. Their core is located just south of the mouth of the Mississippi River and their study site experienced different physical conditions from JPC26. This is because their site is more restricted to Gulf of Mexico ocean dynamics and was significantly influenced by enhanced discharge of the Mississippi River [*Hill et al.*, 2006] during the last glacial cycle. In their methods, *Hill et al.* [2006] did not use a reductive step in their cleaning steps. The reductive step of trace metal cleaning results in a loss of approximately 10% of foraminiferal Mg/Ca [*Barker et al.*, 2003; *Rosenthal et al.*, 2004]. In order to better compare the *Hill et al.* [2006] Orca Basin SST reconstruction to the JPC26 SST reconstruction, an initial reduction of 10% from their Mg/Ca values was calculated. The new raw Mg/Ca values were then converted to SST using equation [2] [*Anand et al.*, 2003].

Hill et al. [2006] suggested that the reconstructed *G. ruber* Mg/Ca – SSTs tracked summertime Antarctic warming from 28 – 45 ka BP rather than millennial-scale temperature changes in the Greenland ice core records. However this result is in conflict with two other SST reconstructions from the North Atlantic during MIS 3 that show an in-phase relationship with Greenland (Figure 9). An alkenone-based SST reconstruction from the Bermuda Rise closely tracked the Greenland ice core record during MIS 3 [*Sachs and Lehman*, 1999] and a foraminiferal fauna-based and alkenone-based SST

reconstruction from the Blake Outer Ridge also broadly tracked Greenland air temperatures during MIS 3 [*Vautravers et al.*, 2004] (Figure 9). Therefore, the Orca Basin SST reconstruction is the only regional SST record that appears to be in phase with warming events in Antarctica during MIS 3. The finding from *Hill et al.* [2006] suggests that the northern Gulf of Mexico may have been isolated from large-scale regional temperature changes in the western tropical Atlantic during MIS 3.

Previous modeling studies suggested high-latitude cooling related to AMOC slowdown is readily transferred to low latitude regions in the Northern Hemisphere through both atmospheric and oceanic processes [*Stouffer et al.*, 2006; *Chiang et al.*, 2008; *Wan et al.*, 2009]. Modeling results show that atmospheric circulation changes associated with AMOC weakening results in a surface cooling in the entire tropical North Atlantic [*Chiang et al.*, 2008; *Wan et al.*, 2009]. In addition, cooler SSTs during stadials in JPC26 probably occurred due to decreased surface current flow from the warm equatorial regions resulting from a slowdown of AMOC. Increased wind strength during stadials may have also resulted in cooler SSTs due to increasing the evaporative heat flux at our study site [*Chiang et al.*, 2008]. During interstadials, an increase in the flow of warm, tropical waters northward due to a stronger AMOC may have caused the observed SST increases in the Florida Straits. Furthermore, a decrease in the surface water evaporative heat flux due to decreased interstadial wind strength may have also resulted in warmer SSTs [*Chiang et al.*, 2008].

A decrease of this magnitude is consistent with modeling studies that show cooler atmospheric temperatures in the tropical North Atlantic in response to a

freshwater-induced weakening of AMOC [*Chiang et al.*, 2008; *Wan et al.*, 2009]. A reduction in AMOC would have reduced northward heat transport, thereby leading to decreases in the calculated JPC26 Mg/Ca – SSTs during H events in JPC 26 due to both atmospheric and oceanic processes [*Chiang et al.*, 2008; *Wan et al.*, 2009]. A decrease in AMOC may also have led to increased surface water evaporative heat flux, thereby decreasing SSTs [*Chiang et al.*, 2008].

7.2. LGM AND MIS 3 Sea Surface Salinity Changes

The calculated $\delta^{18}O_{IVF\text{-}SW}$ record from JPC26 suggests significant surface salinity changes in the Florida Straits across interstadial-stadial transitions from 20 – 35.45 ka BP. Interstadial $\delta^{18}O_{IVF\text{-}SW}$ values tend to be more negative (fresher) and stadial $\delta^{18}O_{IVF\text{-}SW}$ values tend to be more positive (saltier) (Figure 5c). Comparison of the $\delta^{18}O_{IVF\text{-}SW}$ and NGRIP $\delta^{18}O_{ICE}$ records yields a correlation coefficient of -0.34 from 20 – 35.45 ka BP and a correlation coefficient of -0.42 across the highest resolution part of our record from 30.85 – 32.6 ka BP. The abrupt transition to interstadial 5 takes place on the order of 100 years. $\delta^{18}O_{IVF\text{-}SW}$ values peak to near modern values, suggesting an abrupt return to near interglacial conditions (Figure 10a). These light $\delta^{18}O_{IVF\text{-}SW}$ values in the Florida Straits upper water column persist for approximately 500 years before ultimately transitioning back to stadial conditions. Unlike the NGRIP $\delta^{18}O_{ICE}$ temperature record, however, salty stadial conditions after interstadial 5 are short-lived and after ~200 years interstadial-like conditions briefly return to the Florida Straits at

31.8 ka BP. A gradual transition (~550 years) back to stadial conditions then occurs at 31.25 ka BP.

Previous studies showed that a northward shift of the ITCZ results in more precipitation into the Caribbean and the Florida Straits whereas stadial periods are characterized by less precipitation, and therefore high $\delta^{18}O_{IVF\text{-}SW}$ values (increased salinity), and most likely result from a southward displacement of the ITCZ during cold events in the North Atlantic [*Vellinga and Wood*, 2002; *Lohmann*, 2003; *Dahl et al*., 2005; *Zhang and Delworth*, 2005; *Stouffer et al*., 2006; *Schmidt et al.*, 2006]. As annual precipitation increased in the tropical North Atlantic and western Caribbean during interstadials, the regional E – P would also decrease, resulting in lower surface salinity and more negative $\delta^{18}O_{IVF\text{-}SW}$ values in the JPC26 record.

Peterson *et al.* [2000] analyzed the color reflectance and elemental chemistry of a sediment core from the Cariaco Basin, located north of Venezuela. This high-resolution, well-preserved core was characterized by significant decreases in percent reflectance and an increase in counts of iron and titanium during the interstadials. These changes were related to the total amount of rainfall over northern South America, and are thought to result from north-south shifts in the position of the zone of heavy rainfall in the tropics known as the ITCZ [*Peterson et al.*, 2000]. Excursions in the JPC26 $\delta^{18}O_{IVF\text{-}SW}$ reconstruction are similar in timing and duration of the Cariaco Basin Fe record (Figure 11c). Both records suggest greater amounts of precipitation during interstadials and drier stadial conditions in the tropical North Atlantic, which is probably because both of these study sites are directly affected by ITCZ migrations.

The offset in the timing of the observed rapid hydrologic changes in the JPC26 and Cariaco Basin records may result from each record being tuned to a different Greenland ice core record. The JPC26 record is tuned to the NGRIP $\delta^{18}O_{ICE}$ record and the Cariaco record is tuned to the GISP2 $\delta^{18}O_{ICE}$ record (Figure 11, a and c). The transition into interstadial 5 occurs at 32.52 ka BP and full stadial conditions are reached at 32.02 ka BP in the NGRIP $\delta^{18}O_{ICE}$ record. In the GISP2 $\delta^{18}O_{ICE}$ record, however, the transition into interstadial 5 occurs at 32.43 ka BP and full stadial conditions are reached at 31.62 ka BP. If the GISP2 $\delta^{18}O_{ICE}$ and NGRIP $\delta^{18}O_{ICE}$ records were tuned to one another, the hydrologic cycle changes that are present in the JPC26 and Cariaco records would be synchronous.

Additionally, a Southern Hemisphere high-resolution $\delta^{18}O$ speleothem reconstruction from Botuverá Cave in southern Brazil resolved rainfall variations that occurred during the last glacial cycle [*Wang et al.*, 2007] (Figure 1). This cave is located in a prime area to indirectly record ITCZ fluctuations by recording South American Monsoon strength changes, which are affected by the mean position of the ITCZ [*Wang et al.*, 2007]. A southward shift of the ITCZ during stadials is also consistent with reconstructed wet periods in Brazil [*Wang et al.*, 2007] (Figure 12 d). *Wang et al.* [2007] showed that negative $\delta^{18}O$ excursions in cave records from southern Brazil imply a more southerly position of the ITCZ across northern South America during stadials.

Another recently published speleothem record from Peru also showed how the ITCZ affected low latitude Southern Hemisphere monsoon patterns [*Kanner et al.*, 2012]. Similar to the Botuverá Cave record [*Wang et al.*, 2007], this record is anti-

phased with Northern Hemisphere millennial-scale monsoon dynamics and has the appearance of the NGRIP $\delta^{18}O_{ICE}$ record, indicating similar climate forcings (Figure 12, c and d). Therefore, hydrologic changes at this site are also anti-phased with those in the JPC26 $\delta^{18}O_{IVF\text{-}SW}$ record (Figure 12, a, c, and d).

In contrast, *Hill et al.* [2006] concluded that their calculated Orca Basin SST and SSS records tracked summer warming in Antarctica, resulting in melting of the southern margin of the LIS. They argue $\delta^{18}O_{IVF\text{-}SW}$ changes in the Orca Basin were anti-phased with Greenland air temperatures during MIS 3. *Hill et al.* [2006] used a different SST:$\delta^{18}O$ relationship for their calculated JPC26 $\delta^{18}O_{SW}$ record than the JPC26 SST:$\delta^{18}O$ relationship. Their calculation used the *Orbulina universa* high light equation from *Bemis et al.* [1998], whereas the JPC26 $\delta^{18}O_{SW}$ record was calculated by using the *Orbulina universa* low light equation from *Bemis et al.* [1998]. For a better comparison between the Orca Basin and Florida Straits records, their raw data were used to recalculate $\delta^{18}O_{SW}$ using the *Orbulina universa* low light equation [1]. Furthermore, *Hill et al.* [2006] used the *Siddall et al.* [2003] sea level curve to calculate the global ice volume effect on ocean $\delta^{18}O_{SW}$ by using the relationship of a change of 0.083 ‰ per 10 m sea level change [*Adkins and Schrag*, 2001]. To convert their raw data into comparable $\delta^{18}O_{IVF\text{-}SW}$ values similar to the calculated JPC26 $\delta^{18}O_{IVF\text{-}SW}$ record, the *Waelbroeck et al.* [2002] sea level curve was used and the global ice volume change of 0.0875 ‰ per 10 m sea level change was applied [*Schrag et al.*, 2002] to correct for ice volume change (Figure 13 c).

If enhanced melting of the LIS occurred during summer warming in Antarctica

during MIS 2 and 3, as suggested by *Hill et al.* [2006], these effects were localized to the Gulf of Mexico and did not affect our site or other sites in the North Atlantic (Figure 13). This contradicts the hypothesis that outflow from the Mississippi River had a profound impact on AMOC strength, and therefore rapid climate change, during the last glacial [*Flower and Kennett*, 1990; *Clarke et al.*, 2001; *Flower et al.*, 2004, *Hill et al.*, 2006]. No surface freshening events occurred in the Florida Straits during periods of low surface salinity recorded in the Orca Basin $\delta^{18}O_{IVF\text{-}SW}$ record. Therefore, regardless of their findings, the Florida Straits JPC26 $\delta^{18}O_{IVF\text{-}SW}$ reconstruction suggests that Mississippi River discharges may not have had a significant effect on Florida Straits surface salinity change from 20 – 35.45 ka BP.

An alternate source of freshwater into the North Atlantic is iceberg armadas that were released during Heinrich events. Evidence suggests that large amounts of icebergs were discharged into the North Atlantic during Heinrich events [*Heinrich*, 1988; *Bond et al*., 1992; *Bard et al.*, 2000]. The melting of these icebergs could have increased freshwater input and led to upper water column stratification at sites where deepwater forms in the North Atlantic. The geochemical and micropaleontological records from JPC26 show H3 did not have a large impact on SSS in the Florida Straits. It is possible that decreased sedimentation rates across H3 preclude the possibility of constraining hydrographic changes across this event.

In comparison, a substantial decrease in upper water column salinity is recorded across H2 in the *G. ruber* $\delta^{18}O_C$ and $\delta^{18}O_{IVF\text{-}SW}$ records. The beginning of H2 is marked by an extremely short transition to lower salinities and slightly colder SSTs. The large

decrease (~ 0.75 ‰) in $\delta^{18}O_{IVF\text{-}SW}$ values are driven by the *G. ruber* $\delta^{18}O_C$ and probably represent ^{18}O-depleted glacial meltwater entering the oceans from the Mississippi River and entrained in the Loop Current or from meltwater entering the northern North Atlantic that was eventually advected into the subtropical gyre and the Florida Straits.

7.3. *N. dutertrei* Abundance Record

N. dutertrei generally inhabit the more productive areas of tropical and subtropical regions of the oceans and are most dense near the deep chlorophyll maximum [*Fairbanks et al.*, 1982; *Curry et al.*, 1983; *Ortiz et al.*, 1995]. They also inhabit regions of the oceans directly affected by nutrient-rich, low salinity river water [*Maslin and Burns*, 2000; *Schmuker and Schiebel*, 2002; *Rasmussen and Thomsen*, 2012]. Previous paleoceanographic studies have linked the downcore abundance of *N. dutertrei* to eutrophic and/or fresher conditions thought to result from continental meltwater pulses [*Ruddiman*, 1971; *Cullen*, 1981; *Fairbanks et al.*, 1982; *Curry et al.*, 1983; *Rasmussen and Thomsen*, 2012].

The new JPC26 *N. dutertrei* abundance record supports our calculated $\delta^{18}O_{IVF\text{-}SW}$ record as a robust proxy for SSS change in the Florida Straits. Comparison of the $\delta^{18}O_{IVF\text{-}SW}$ and *N. dutertrei* abundance records yields a correlation coefficient of -0.25 (Figure 5, d and e). Although the correlation coefficient does not signify a strong relationship between these two variables across the entire record, they are extremely similar in shape during periods of fresher conditions. Furthermore, fewer *N. dutertrei*

were observed during periods of heavier $\delta^{18}O_{IVF\text{-}SW}$ values. Significant increases in the amount of *N. dutertrei* are observed during interstadials 7, 6, 5, and 4 (Figure 5e), consistent with the fresher conditions implied by the calculated $\delta^{18}O_{IVF\text{-}SW}$ record at these times. Interstadial 3 is associated with a very small increase in *N. dutertrei*, but no increase is observed across interstadial 2. In general, much fewer *N. dutertrei* are present during stadial periods; in fact, they are absent in the stadials just before interstadial 5 and H2.

The sharp increase in the number of *N. dutertrei* across interstadial 5 could indicate a rapid freshening at this time, consistent with the negative excursion in the $\delta^{18}O_{IVF\text{-}SW}$ values. There is no increase across H3, consistent with a small $\delta^{18}O_{IVF\text{-}SW}$ change across the event. H2 is punctuated by a significant increase in the population of *N. dutertrei*, which may have resulted from melting icebergs/ice sheets and advection of these fresh waters to the Florida Straits from either the Mississippi River or the northern North Atlantic.

7.4. *G. ruber* Ba/Ca

The previous discussion of the calculated $\delta^{18}O_{IVF\text{-}SW}$ record from JPC26 is based on the assumption that evaporation and precipitation are the only active variables affecting $\delta^{18}O_{IVF\text{-}SW}$. However, it is possible that $\delta^{18}O$-depleted glacial meltwater discharged from the Laurentide ice sheet influenced the calculated $\delta^{18}O_{IVF\text{-}SW}$ values of MIS 2 and 3, especially during the abrupt warming events any associated melting of

continental ice sheets [*Hill et al.*, 2006; *Schmidt and Lynch-Stieglitz*, 2011]. Because riverine waters have elevated barium concentrations, an increased influence of meltwater should be characterized by both isotopically light $\delta^{18}O_{IVF\text{-}SW}$ values and high Ba/Ca ratios in *G. ruber*.

Due to the proximity of the Florida Straits to the Mississippi River and the dynamics of Gulf of Mexico (GOM) ocean circulation patterns, the potential exists that increased discharge into the GOM may have been recorded in the surface-dwelling planktonic foraminifera *Globigerinoides ruber* Ba/Ca ratios during the last glacial cycle. The largest Mississippi River flood in recent times occurred in 1993, and properties of this discharge were documented by *Ortner et al.* [1995] and *Gilbert et al*. [1996]. *Hu et al.* [2005] also tracked a Mississippi River-sourced freshwater plume to the Florida Straits and Gulf Stream during late Summer/early Autumn in 2004 and observed a much higher chlorophyll abundance but only slightly higher nutrient concentrations. The unique physical conditions that must be satisfied to entrain Mississippi River water and transport it to the Florida Keys are a northward position of the Loop Current, highly stratified surface waters, high Mississippi River discharge rates, and eastward winds [*Ortner et al.*, 1995; *Gilbert et al.*, 1996; *Hu et al.*, 2005].

Schmidt and Lynch-Stieglitz [2011]'s deglacial Ba/Ca record from JPC26 suggested that meltwater pulses affected salinity in the Florida Straits during the deglacial, and that these events were linked to enhanced melting of the Laurentide ice sheet. Therefore, periods of abrupt warming (*e.g.*, interstadials) may be correlated to maxima of Ba/Ca ratios in the planktonic foraminiferal record because of enhanced

melting of the North American continental ice sheet.

However, the reconstructed Florida Straits Ba/Ca record from 20 to 35.45 ka BP does not suggest increased riverine input affected salinity during interstadials. Comparison between the reconstructed Ba/Ca and $\delta^{18}O_{IVF\text{-}SW}$ records yields a correlation coefficient of only 0.18 and comparison of the reconstructed Ba/Ca and *N. dutertrei* abundance records yields a correlation coefficient of -0.37. This would suggest that more *N. dutertrei* are present (fresher conditions) during periods of lower barium concentrations (reduced riverine input). If increased riverine input into the Gulf of Mexico (higher Ba/Ca) were the driver of the surface salinity decreases in the Florida Straits, a positive correlation would be expected with *N. dutertrei* abundance. Therefore, it is unlikely that changes in the JPC26 Ba/Ca record are driven by variations in meltwater input to the Gulf of Mexico during MIS 3.

An alternate potential source of dissolved barium to continental shelves is coastal sediments [*Moore*, 1999]. Sea level rise may cause previously adsorbed barium on open shelf sediments to desorb as a response to coming into contact with saline waters [*Moore and Shaw*, 1997; *Hall and Chan*, 2004]. This mechanism of saltwater encroachment and resultant release of dissolved barium in groundwater has been reported from Floridian freshwater aquifers [*Moore and Shaw*, 1998]. However, from 35.45 – 20 ka BP, sea level was decreasing [*Yokoyama et al.*, 2000; *Waelbroeck et al.*, 2002], so there should be minimal influence from barium in coastal sediments.

Another factor that may potentially influence the *G. ruber* Ba/Ca record is enhanced weathering due to sea level changes. A correlation coefficient of -0.79 was

calculated when comparing the JPC26 Ba/Ca record to the spliced *Yokoyama et al.* [2000] and *Waelbroeck et al.* [2002] sea level curves (Figure 7, c and d), indicating higher Ba/Ca ratios during sea level lowstands. This suggests that a relationship may exist between Ba/Ca ratios from the Florida Straits and eustatic sea level changes during MIS 2 and 3. Because sea level was decreasing relative to modern from 35.45 – 20 ka BP [*Yokoyama et al.*, 2000; *Waelbroeck*, 2002], there would have been an associated increase in the total area of shelf sediments that were exposed to the air and therefore atmospheric processes. Enhanced erosion of recently exposed shelf sediments may have played a role in the coeval changes between sea level and planktonic foraminiferal Ba/Ca ratios.

As noted above, a substantial decrease in upper water column salinity is recorded across H2 in the *G. ruber* $\delta^{18}O_C$ and $\delta^{18}O_{IVF\text{-}SW}$ records (Figure 5, a and d). Simultaneous increases in the abundance of *N. dutertrei* during H2 also suggest that the upper water column freshened at this time. However, the *G. ruber* Ba/Ca record shows no positive anomaly during H2. Because glacial meltwater from the Mississippi River would also have elevated barium concentrations, it is unlikely that the source of the isotopically light $\delta^{18}O_{IVF\text{-}SW}$ values during H2 resulted from a freshwater discharge into the northern Gulf of Mexico. Ultimately, the source for the isotopically light waters in the subtropical Atlantic at this time may have been in the high-latitudes, originating from the iceberg discharge associated with H2.

Importantly, the JPC26 Ba/Ca record suggests that millennial-scale meltwater injections into the Gulf of Mexico did not significantly influence surface salinity in the

Florida Straits from 20 – 35.45 ka BP. Therefore, the calculated $\delta^{18}O_{IVF\text{-}SW}$ values are probably not affected by local ^{18}O-depleted glacial meltwater routed through the Mississippi River and eventually to the Florida Straits. Instead, the calculated $\delta^{18}O_{IVF\text{-}SW}$ record most likely represents regional changes in E – P in the western tropical Atlantic and Caribbean.

7.5. Interstadial 4.2

Interestingly, both the calculated $\delta^{18}O_{IVF\text{-}SW}$ record and the JPC26 *N. dutertrei* abundance record from JPC26 suggest a return to interstadial-like conditions in the Florida Straits at 31.8 ka BP, shortly after the start of the stadial between interstadials 5 and 4 at 32 ka BP (yellow shaded bar on Figures 5, 7, 10, 11, and 12). However, there is no corresponding interstadial at this time in the NGRIP $\delta^{18}O_{ICE}$ record (Figure 5f). Furthermore, this return to interstadial-like conditions was not isolated to the Florida Straits. It is also observed in the Cariaco Basin Fe record [*Peterson et al.*, 2000] (Figure 11c) and in the Southern Hemisphere cave record from Peru [*Kanner et al.*, 2012] (Figures 11d and12c). As shown in Figure 11, there is a slight lead in the timing of this event between the Cariaco Basin Fe record [*Peterson et al.*, 2000] and the JPC26 record. This may be due to the fact that the Cariaco Basin record is tuned to the GISP II $\delta^{18}O_{ICE}$ record used in this study, as discussed above. Tuning the Cariaco Basin record to the NGRIP $\delta^{18}O_{ICE}$ record would result in a more synchronous change with the JPC26 $\delta^{18}O_{IVF\text{-}SW}$ and *N. dutertrei* abundance records during this event.

A northward migration of the ITCZ to an interstadial-like position would result in greater amounts of precipitation in northern South America and Central America [*e.g., Peterson et al.*, 2000; *Vellinga and Wood*, 2002; *Lohmann*, 2003; *Dahl et al*., 2005; *Zhang and Delworth*, 2005; *Stouffer et al*., 2006; *Correa-Metrio et al., 2012*] and the Florida Straits, consistent with the return to fresher conditions in the JPC26 $\delta^{18}O_{IVF\text{-}SW}$ record at 31.8 ka BP. This short-lived, rebound of the ITCZ to a more northward position would have also resulted in drier conditions in the southern tropics/subtropics, explaining shift to heavier oxygen isotope values in the Peru speleothem record (Figure 11d) [*Kanner et al.*, 2012]. Because this brief climate event is not present in the Greenland ice core records, it seems likely this return to interstadial-like conditions was limited to the tropics. If this event was only experienced in the tropics as we speculate, it suggests a driver of tropical hydrological cycle dynamics independent of high-latitude climate change at this time.

7.6. Estimating Geostrophic Currents from $\delta^{18}O$ in Benthic Foraminifera

Several attempts have been made to reconstruct AMOC strength directly or indirectly during the last glacial cycle in order to determine its influence on climate [*Lynch-Stieglitz et al.*, 1999a; *McManus et al.*, 2004; *Piotrowski et al.*, 2005; *Lund et al.*, 2006; *Praetorius et al.*, 2008; *Lynch-Stieglitz et al.*, 2011]. These studies link a reduction in inferred AMOC strength to cold temperatures in the northern hemisphere utilizing different proxies. Although glacial-interglacial and some high-frequency

events are resolvable, an extremely high-resolution record of AMOC variability spanning MIS 2 and 3 currently does not exist.

The Florida Straits is located where reconstructions of geostrophic currents can be used to infer past changes in Florida Current transport related to AMOC strength. *Lynch-Stieglitz et al.* [1999b] pioneered a study that showed that the $\delta^{18}O$ in modern benthic foraminifera (*Planulina spp.* and *Cibicidoides spp.*) reflect the density of waters on either margin of the Florida Straits (Florida and Bahamas platforms). The flow of water through the Florida Straits is geostrophic, with the Coriolis force (a function of latitude and water velocity) being balanced by a pressure gradient that is faithfully recorded in benthic $\delta^{18}O_C$ [*Lynch-Stieglitz et al.*, 1999b; *Lund et al.*, 2006; *Lynch-Stieglitz et al.*, 2011]. Increased flow results in a greater cross-straits density gradient, while a reduction in Florida Current transport results in a smaller cross-straits density gradient.

Lynch-Stieglitz et al. [2011] used JPC26 to reconstruct Florida Current transport across the last deglacial and found that the Florida Current was significantly reduced during the Younger Dryas cold period. This weakening would have resulted in a reduction in heat transport of warm, equatorial waters to the high latitudes, and inducing significant cooling in the North Atlantic.

Lynch-Stieglitz et al. [in prep] also developed companion benthic $\delta^{18}O_C$ records from both margins of the Florida Straits in order to reconstruct past changes in Florida Current transport from 20 – 35.5 ka BP. Because $\delta^{18}O_C$ changes on the Bahamas Margin primarily reflect sea level changes and changes in temperature [*Lynch-Stieglitz et al.*, in

prep], changes in the ice-volume corrected benthic $\delta^{18}O_C$ record from the Florida Margin in core JPC26 can be used to infer Florida current and AMOC strength during MIS 3. Furthermore, the *G. ruber* record in JPC26 reflects atmospheric circulation changes, as discussed above. Therefore, it is possible to infer the timing of atmospheric and ocean circulation changes across the abrupt climate events from the LGM to 35.45 ka BP.

It is clear the transition into interstadial 5 is marked by an initial freshening recorded in the *N. dutertrei* abundance record (Figures 10b and 11b). The calculated $\delta^{18}O_{IVF\text{-}SW}$ and the benthic $\delta^{18}O_C$ values lag the *N. dutertrei* abundance increase by approximately 75 years and 8 cm deeper in the core. The actual timing of the *G. ruber* $\delta^{18}O_{IVF\text{-}SW}$ rise can be questioned because of the uncertainties involved in calculating $\delta^{18}O_{IVF\text{-}SW}$. Errors associated with instrumental analyses and errors associated with empirical calculations (equations 1 and 2) are compounded when calculating $\delta^{18}O_{IVF\text{-}SW}$. Therefore, more confidence is placed on the timing of the *N. dutertrei* abundance record as a proxy for past salinity change because of the simplicity of that calculation. As shown in Figures 5 and 10, the *N. dutertrei* abundance record closely resembles the calculated $\delta^{18}O_{IVF\text{-}SW}$ record, which is to be expected if *N. dutertrei* are sensitive to upper ocean salinity changes. The *N. dutertrei* abundance record leads the benthic $\delta^{18}O_{IVF\text{-}C}$ change on the transition into interstadial 5 (Figure 10). This suggests that tropical atmospheric reorganizations may lead oceanic circulation (AMOC) changes on the transition into the interstadials during the last glacial cycle. This lead in atmospheric circulation changes is similar to *Schmidt and Lynch-Stieglitz* [2011]'s finding that atmospheric changes occurred before oceanic changes during the transition out of the

Younger Dryas cold period.

Otto-Bliesner and Brady [2010] used a coupled ocean-atmosphere climate model under LGM boundary conditions and their results suggested that atmospheric responses led oceanic circulation changes during the transition out of the Younger Dryas. In their model, the ITCZ rebounded to its northward interstadial position before AMOC strengthened after a freshwater induced weakening of AMOC [*Otto-Bliesner and Brady*, 2010]. They suggested that this response may have been viable under MIS 3 conditions.

In contrast, the transition to stadial conditions is approximately synchronous; no lead/lag response is observed between the benthic $\delta^{18}O_{IVF\text{-}C}$ record and the *N. dutertrei* abundance record on the transition into the stadial around 32 ka BP (Figure 10). This implies that tropical hydrologic cycle changes were synchronous with AMOC changes on the transition into this stadial event. This is also consistent with *Schmidt and Lynch-Stieglitz* [2011]'s findings on the transition into the YD.

Another major abrupt climate event recorded by the benthic and planktonic foraminifera occurred across H2. Based on the JPC26 benthic $\delta^{18}O_{IVF\text{-}C}$ record Florida Straits transport decreased during the onset of H2, suggesting that AMOC was reduced at this time. This oceanic response occurs ~220 years before and 4 cm deeper in the core than the surface ocean response that was recorded in the JPC26 calculated $\delta^{18}O_{IVF\text{-}SW}$ and *N. dutertrei* abundance records (Figure 14). The decrease in $\delta^{18}O_{IVF\text{-}SW}$ values and the increase in *N. dutertrei* abundance was most likely caused by the advection of low salinity waters from the high-latitude North Atlantic into the Florida Straits.

Subtropical gyre currents may have directed these low salinity waters from the North Atlantic to the Florida Straits, resulting in the $\delta^{18}O_{IVF\text{-}SW}$ decrease (freshening) and the *N. dutertrei* abundance increase.

8. CONCLUSIONS

Abrupt sea surface temperature and hydrologic cycle variations in the Florida Straits were linked to temperature variations recorded in the NGRIP $\delta^{18}O_{ICE}$ record from 20 – 35.45 ka BP. The millennial-scale climate oscillations of MIS 3 known as Dansgaard-Oeschger cycles and Heinrich events, were recorded in the foraminiferal geochemical and faunal abundance proxies analyzed in core JPC26. Some interstadials are associated with increased *G. ruber* Mg/Ca ratios and decreased $\delta^{18}O_{IVF\text{-}SW}$ values, suggesting warm conditions and reduced surface salinities (decreased E – P) in the Florida Straits, whereas stadials are generally marked by more positive $\delta^{18}O_{IVF\text{-}SW}$ values and lower Mg/Ca ratios reflecting cooler, saltier conditions (increased E – P).

Based on the *G. ruber* record from 20 – 35.45 ka BP, long-term changes in the barium concentration of Florida Straits surface waters are not linked to enhanced riverine input into the Gulf of Mexico, but instead track sea level changes. Our results indicate that there is no evidence for increased Mississippi River meltwater influence on surface waters in the Florida Straits from 20 – 35.45 ka BP. These findings contradict the previous hypothesis that enhanced discharge from the Mississippi River affected AMOC strength and played an important role in abrupt climate changes during the last glacial cycle [*Flower and Kennett*, 1990; *Clark et al.*, 2001].

Furthermore, Heinrich events 2 and 3 affected the Florida Straits in different ways. H2 conditions were extremely fresh and cooler and the benthic $\delta^{18}O_{IVF\text{-}C}$ record suggests that the Florida Current weakened, whereas no substantial changes in the

Florida Straits salinity or Florida Current transport decrease through H3.

Comparison of the planktonic-based $\delta^{18}O_{IVF\text{-}SW}$ reconstruction and the *N. dutertrei* abundance record from 20 – 35.45 ka BP with the benthic $\delta^{18}O_{IVF\text{-}C}$ record in core JPC26 suggests that reorganizations of the tropical hydrologic cycle may have occurred before large-scale oceanic circulation changes (*e.g.*, AMOC) during the transition into interstadial 5. Whether or not the lead in atmospheric processes occurred during each transition to millennial-scale interstadial events of MIS 2 and 3 is still unknown, although a recent proxy reconstruction from the Florida Straits using the same core in this study showed a lead in atmospheric circulation changes before the Florida Current fully recovered at the end of the YD at about 11.6 ka BP [*Schmidt and Lynch-Stieglitz*, 2011]. In addition, modeling results also suggest this sequence of events during the transition into interstadial warm periods during the last glacial cycle [*Otto-Bliesner and Brady*, 2010]. Decreased sedimentation rates across much of the record, relative to interstadial 5 sedimentation rates, preclude the ability to resolve each millennial-scale event with high confidence. However, there is a growing body of evidence [*Benway et al.*, 2006; *Leduc et al.*, 2007; *Otto-Bliesner and Brady*, 2010; *Schmidt and Lynch-Stieglitz*, 2011; *this study*] that suggests the tropics played a very important role in the initiation of abrupt warming events (interstadials) of MIS 2 and 3.

The rapid hydrologic cycle changes recorded in JPC26 most likely reflect changes in the position and strength of the ITCZ on millennial time scales and are consistent with several other proxy reconstructions for this time interval [*Peterson et al.*, 2000; *NGRIP members*, 2004; *Correa-Metrio et al.,* 2012; *Kanner et al.*, 2012]. Our

results suggest that the tropical Atlantic hydrologic cycle plays an active role in millennial-scale climate change.

REFERENCES

Adkins, J.F., and D.P. Schrag, 2001, Pore fluid constraints on the deep ocean temperature and salinity during the last glacial maximum, *Geophysical Research Letters*, *28*, 771 – 774.

Adkins, J.F., K. McIntyre, and D.P. Schrag, 2002 The Salinity, Temperature, and $\delta^{18}O$ of the Glacial Deep Ocean, *Science*, *298*, 1769 – 1773.

Alley, R.B., and P.U. Clark, 1999, The deglaciation of the Northern Hemisphere: A Global Perspective, *Annual Review of Earth and Planetary Sciences*, *27*, 149 – 182.

Anand, P., H. Elderfield, and M. H. Conte, 2003, Calibration of Mg/Ca thermometry in planktonic foraminifera from a sediment trap time series, *Paleoceanography*, *18*, 2, 1 – 15.

Antonov, J.I., D. Seidov, T.P. Boyer, R.A. Locarnini, A.V. Mishonov, and H.E. Garcia (Eds.), 2010, *World Ocean Atlas 2009*, 184pp., U.S. Government Printing Office, Washington, D.C.

Arbuszewski, J., P. deMenocal, A. Kaplan, and E.C. Farmer, 2010, On the fidelity of shell-derived $\delta^{18}O_{seawater}$ estimates, *Earth and Planetary Science Letters*, 300, 185 – 196.

Bard, E., F. Rostek, J.L. Turon, and S. Gendreau, 2000, Hydrological Impact of Heinrich Events in the Subtropical Northeast Atlantic, *Science*, *289*, 1321 – 1324.

Barker, S., M. Greaves, and H. Elderfield, 2003, A study of cleaning procedures used for foraminferal Mg/Ca paleothermometry, *Geochemistry Geophysics Geosystems*, *4*, 9, 2003GC000559.

Barker, S., I. Cacho, H. Benway, and K. Tachikawa, 2005, Planktonic foraminiferal Mg/Ca as a proxy for past oceanic temperatures: a methodological overview and data compilation for the Last Glacial Maximum, *Quaternary Science Reviews*, *24*, 821 – 834.

Bemis, B.E., H.J. Spero, J. Bijma, and D.W. Lea, 1998, Reevaluation of the oxygen isotopic composition of planktonic foraminifera: Experimental results and revised paleotemperature equations, *Paleoceanography*, *13*, 2, 150 – 160.

Benway, H.M., A.C. Mix, B.A. Haley, and G.P. Klinkhammer, 2006, Eastern Pacific Warm Pool paleosalinity and climate variability: 0 – 30 kyr, *Paleoceanography*,

PA3008.

Berger, W.H., 1968, Planktonic Foraminifera: selective solution and paleoclimatic interpretation, *Deep-Sea Research*, *15*, 31 – 43.

Bond, G., H. Heinrich, W. Broecker, L. Labeyrie, J. McManus, J. Andrews, S. Huon, R. Jantschik, S. Clasen, C. Simet, K. Tedesco, M. Klas, G. Bonani, and S. Ivy, 1992, Evidence for massive discharges of icebergs into the North Atlantic Ocean during the last glacial period, *Nature*, *360*, 245 – 249.

Boyle, E., 2000, Is ocean thermohaline circulation linked to abrupt stadial/interstadial transitions? *Quaternary Science Reviews*, *19*, 255 – 272.

Broecker, W.S., G. Bond, M. Klas, G. Bonani, and W. Wolfli, 1990, A Salt Oscillator in the Glacial Atlantic? 1. The Concept, *Paleoceanography*, *5*, 4, 469 – 477.

Brown, S.J., and H. Elderfield, 1996, Variations in Mg/Ca and Sr/Ca ratios of planktonic foraminifera caused by postdepositional dissolution: Evidence of shallow Mg-dependent dissolution, *Paleoceanography*, *11*, 5, 543 – 551.

Cane, M., and A.C. Clement, 1999, A role for the tropical Pacific coupled ocean-atmosphere system on Milankovitch and millennial timescales. Part II: Global Impacts, *Mechanisms of Global Climate Change at Millennial Time Scales*, *Geophysical Monograph 112*, 373 – 383.

Carlson, A.E., D.W. Oppo, R.E. Came, A.N. LeGrande, L.D. Keigwin, and W.B. Curry, 2008, Subtropical Atlantic salinity variability and Atlantic meridional circulation during the last deglaciation, *Geology*, *36*, 991 – 994.

Charles, C.D., and R.G. Fairbanks, 1990, Glacial to interglacial changes in the isotopic gradients of southern ocean surface water, in *Geological History of the Polar Oceans: Arctic Versus Antarctic*, edited by U. Bleil and J. Thiede, pp. 519 – 538, Kluwer Acad., Dordrecht, Netherlands.

Charles, C.D., D. Rind, J. Jouzel, R. Koster, and R.G. Fairbanks, 1994, Glacial-interglacial changes in moisture sources for Greenland: Influences on the ice core record of climate, *Science*, *263*, 508 – 511.

Chiang, J.C.H., W. Cheng, and C.M. Bitz, 2008, Fast teleconnections to the tropical Atlantic sector from Atlantic thermohaline adjustment, *Geophysical Research Letters*, *35*, L07704.

Clark, P.U., S.J. Marshall, G.K.C. Clarke, S.W. Hostetler, J.M. Licciardi, and J.T. Teller, 2001Freshwater Forcing of Abrupt Climate Change During the Last Glaciation, *Science*, *293*, 283 – 287.

Clement A.C., and L.C. Peterson, 2008, Mechanisms of Abrupt Climate Change of the last Glacial Period, *Reviews of Geophysics*, *46*, RG4002.

Coffey, M., F. Dehairs, O. Collette, G. Luther, T. Church, and T. Jickells, 1997, The behavior of dissolved barium in estuaries, *Estuarine, Coastal and Shelf Science*, *45*, 113 – 121.

Correa-Metrio, A., M.B. Bush, K.R. Cabrera, S. Sully, M. Brenner, D.A. Hodell, J. Escobar, and T. Guilderson, 2012, Rapid climate change and no-analog vegetation in lowland Central America during the last 86,000 years, *Quaternary Science Reviews*, doi:10.1016/j.quascierev.2012.01. 025.

Craig, H., and L.I. Gordon, 1965, in *Stable Isotopes in Oceanographic Studies and Paleotemperatures* (ed. Tongiorgi, E.), CNR, Pisa, 9 – 130.

Cramer, B.S., K.G. Miller, P.J. Barnett, and J.D. Wright, Late Cretaceous-Neogene trends in deep ocean temperature and continental ice volume: Reconciling records of benthic foraminiferal geochemistry ($\delta^{18}O$ and Mg/Ca) with sea level history, *Journal of Geophysical Research*, *116*, C12023.

Cullen, J.L., 1981, Microfossil evidence for changing salinity patterns in the Bay of Bengal over the last 20 000 years, *Palaeogeography, Palaeoclimatology, Palaeoecology*, *35*, 315 – 356.

Dahl, K., A.J. Broccoli, and R.J. Stouffer, 2005, Assessing the role of North Atlantic freshwater forcing in millenial scale climate variability: a tropical Atlantic perspective, *Climate Dynamics*, *24*, 325 – 346.

Dansgaard, W., S.J. Johnsen, J. Møller, H.C. Oersted, and C.C. Langway, Jr., 1969, One thousand centuries of climatic record from Camp Century on the Greenland Ice Sheet, *Science*, *166*, 377 – 380.

Dansgaard, W., S.J. Johnsen, H.B. Clausen, D. Dahl-Jensen, N.S. Gundestrup, C.U. Hammer, C.S. Hvidberg, J.P. Steffensen, A.E. Sveinbjörnsdottir, J. Jouzel, and G. Bond, 1993, Evidence for general instability, of past climate from a 250-kyr ice-core record, *Nature*, *364*, 218 – 220.

Dekens, P.S., D.W. Lea, D.K. Pak, and H.J. Spero, 2002, Core top calibration of Mg/Ca in tropical foraminifera: Refining paleotemperature estimation, *Geochemistry Geophysics Geosystems*, *3*, 4, GC000200.

Dueñas-Bohórquez, A., R.E. da Rocha, A. Kuroyanagi, J. Bijma, and G.-J. Reichart, 2009, Effect of salinity and seawater calcite saturation state on Mg and Sr incorporation in cultured planktonic foraminifera, *Marine Micropaleontology*, *73*, 178 – 189.

Duplessy, J.C., C. Lalou, and A.C. Vinot, 1970, Differential Isotopic Fractionation in Benthic Foraminifera and Paleotemperatures Reassessed, *Science*, *168*, 250 – 251.

Edmond, J. M., E.D. Boyle, D. Drummond, B. Grant, and T. Mislick, 1978, Desorption of barium in the plume of the Zaire (Congo) river, *Netherlands Journal of Sea Research*, *12*, 3-4, 324 – 328.

Elderfield, H., and G. Ganssen, 2000, Past temperature and $\delta^{18}O$ of surface ocean waters inferred from foraminferal Mg/Ca ratios, *Nature*, *405*, 442 – 445.

EPICA Community Members, 2006, One-to-one coupling of glacial climate variability in Greenland and Antarctica, *Nature*, *444*, 195 – 198.

Epstein, S., and T. Mayeda, 1953, Variation of O^{18} content of waters from natural sources, *Geochimica et Cosmochimica Acta*, 4, 213 – 224.

Fairbanks, R.G., M. Sverdlove, R. Free, P.H. Wiebe, and A.W.H. Bé, 1982, Vertical distribution and isotopic fractionation of living planktonic foraminifera from the Panama Basin, *Nature*, *298*, 841 – 844.

Farrell, J.W., and W.L. Prell, 1989, Climatic Change and $CaCO_3$ Preservation: An 800,000 Year Bathymetric Reconstruction from the Central Equatorial Pacific Ocean, *Paleoceanography*, *4*, 4, 447 – 466.

Fatela, F., and R. Taborda, 2002, Confidence limits of species proportions in microfossil assemblages, *Marine Micropaleontology*, *45*, 169 – 174.

Ferguson, J.E., G.M. Henderson, M. Kucera, and R.E.M. Rickaby, 2008, Systematic change of foraminiferal Mg/Ca ratios across a strong salinity gradient, *Earth and Planetary Science Letters*, *265*, 153 – 166.

Flower, B.P., and J.P. Kennett, 1990, The Younger Dryas Cool Episode in the Gulf of Mexico, *Paleoceanography*, *5*, 6, 949 – 961.

Flower, B.P., D.W. Hastings, H.W. Hill, and T.M. Quinn, 2004, Phasing of deglacial warming and Laurentide Ice Sheet meltwater in the Gulf of Mexico, *Geology*, *32*, 7, 597 – 600.

Fratantoni, P.S., T.N. Lee, G.P. Podesta, and F.E. Müller-Karger, 1998, The influence of Loop Current perturbations on the formation and evolution of Tortugas eddies in the southern Straits of Florida, *Journal of Geophysical Research*, *103*, C11, 759 – 779.

Gilbert, P.S., T.N. Lee, and G.P. Podestá, 1996, Transport of anomalous low-salinity waters from the Mississippi River flood of 1993 to the Straits of Florida, *Continental Shelf research*, *16*, 8, 1065 – 1085.

Hall, J., and L.-H. Chan, 2004, Ba/Ca in Neoglogoquadrina pachyderma as an indicator of deglacial meltwater discharge into the western Arctic Ocean, *Paleoceanography*, *19*, PA000910.

Hanor. J.S., and L.-H. Chan, 1977, Non-conservative behavior of barium during mixing of Mississippi River and Gulf of Mexico waters, *Earth and Planetary Science Letters*, *37*, 242 – 250.

Hastings, D. A., A.D. Russell, and S.R. Emerson, 1998, Foraminiferal magnesium in *Globigerinoides sacculifer* as a paleotemperature proxy, *Paleoceanography*, *13*, 2, 161 – 169.

Heinrich, H., 1988, Origin and Consequences of Cyclic Ice Rafting in teh Northeast Atlantic Ocean during the Past 130,000 years, *Quaternary Research*, *29*, 142 – 152.

Hemming, S.R., 2004, Heinrich Events: Massive Late Pleistocene Detritus Layers of the North Atlantic and Their Global Climate Imprint, *Review of Geophysics*, *42*, RG1005.

Hill, H.W., T.M. Quinn, D.J. Hollander, and T.P. Guilderson, 2006, Laurentide Ice Sheet meltwater and abrupt climate change during the last glaciation, *Paleoceanography*, *21*, PA1006.

Hönisch, B., K.A. Allen, A.D. Russell, S.M. Eggins, J. Bijma, H.J. Spero, D.W. Lea, and J. Yu, 2011, Planktic foraminifers as recorders of seawater Ba/Ca, *Marine Micropaleontology*, *79*, 52 – 57.

Howell, P, N. Pisias, J. Balance, J. Baughman, and L. Ochs, 2006, ARAND Time-Series Analysis Software, Brown University, Providence RI.

Hu, C., J.R. Nelson, E. Johns, Z. Chen, R.H. Weisberg, and F.E. Müller-Karger, 2005, Mississippi River water in the Florida Straits and in the Gulf Stream off Georgia in summer 2004, *Geophysical Research Letters*, *32*, L14606.

Hughen, K., S. Lehman, J. Southon, J. Overpeck, O. Marchal, C. Herring, and J. Turnbull, 2004, C-14 activity and global carbon cycle changes over the past 50,000 years, *Science*, *303*, 202 – 207.

Jackson, C., 2000, Sensitivity of stationary waver amplitude to regional changes in Laurentide ice sheet topography in single-layer models of the atmosphere, *Journal of Geophysical Research*, *105*, D19, 24,443 – 24,454.

Kanner, L.C., S.J. Burns, H. Cheng, and R.L. Edwards, 2012, High-Latitude Forcing of the South American Summer Monsoon During the Last Glacial, *Science*, *335*, 570 – 573.

Kennett, J. P., K. Elmstrom, and N. Penrose, 1985, The last deglaciation in Orca Basin, Gulf of Mexico: high-resolution planktonic foraminiferal changes, *Paleogeography, Palaeoclimatology, Palaeoecology*, *50*, 189 – 216.

Kisakürek, A. Eisenhauer, F. Böhm, D. Garbe-Schönberg, and J. Erez, 2008, Controls on shell Mg/Ca and Sr/Ca in cultured planktonic foraminiferan, *Globigerinoides ruber* (white), *Earth and Planetary Science Letters*, *273*, 260 – 269.

Krebs, U., and A. Timmermann, 2007a, Fast advective recovery of the Atlantic meridional overturning circulation after a Heinrich event, *Paleoceanography*, *22*, PA1220.

Krebs, U., and A. Timmermann, 2007b, Tropical air-sea interactions accelerate the recovery of the Atlantic Overturning Meridional Overturning Circulation after a major shutdown, *Journal of Climate*, *20*, 4940 – 4956.

Lea, D.W., and H.J. Spero, 1994, Assessing the reliability of paleochemical tracers: Barium uptake in the shells of planktonic foraminifera, *Paleoceanography*, *9*, 3, 445 – 452.

Lea, D.W., and P.A. Martin, 1996, A rapid mass spectrometric method for the simultaneous analysis of barium, cadmium, and strontium in foraminifera shells, *Geochimica et Cosmochimica Acta*, *60*, 16, 3143 – 3149.

Lea, D. W., T.A. Mashiotta, and H.J. Spero, 1999, Controls on magnesium an strontium uptake in planktonic foraminifera determined by live culturing, *Geochimicia et Cosmochimica Acta*, *63*, 16, 2369 – 2379.

Lea, D.W., D.K. Pak, and H.J. Spero, 2000, Climate Impact of Late Quaternary Equatorial Pacific Sea Surface Temperature Variations, *Science*, *289*, 1719 – 1724.

Lear, C.H., H. Elderfield, and P.A. Wilson, 2000, Cenozoic Deep-Sea Temperatures and Global Ice Volumes from Mg/Ca in Benthic Foraminiferal Calcite, *Science*, *287*, 269 – 272.

Leduc, G., L. Vidal, K. Tachikawa, F. Rostek, C. Sonzogni, L. Beaufort, and E. Bard, 2007, Moisture transport across Central America as a positive feedback on abrupt climate changes, *Nature*, *445*, 908 – 911.

Locarnini, R. A., 2006, Volume 1: Temperature, S. Levitus, Ed. NOAA Atlas NESDIS 61, U.S. Government Printing Office, Washington, D.C., 182 pp.

Lohmann, G., 2003, Atmospheric and oceanic freshwater transport during weak Atlantic overturning circulation, *Tellus*, *55A*, 5, 438 – 449.

Lohmann, G., and S. Lorenz, 2000, On the hydrological cycle under paleoclimatic conditions as derived from AGCM simulations, *Journal of Geophysical Research*, *105*, D13, 17,417 – 17,436.

Lund, D.C., J. Lynch-Stieglitz, and W.B. Curry, 2006, Gulf Stream density structure and transport during the past mellennium, *Nature*, *444*, 601 – 604.

Lund, D.C., and W. Curry, 2006, Florida Current surface temperature and salinity variability during the last millennium, *Paleoceangraphy*, *21*, PA2009.

Lynch-Stieglitz, J., W.B. Curry, and N.C. Slowey, 1999a, Weaker Gulf Stream in the Florida Straits during the Last Glacial Maximum, *Nature*, *402*, 644 – 648.

Lynch-Stieglitz, J., W.B. Curry, and N.C. Slowey, 1999b, A geostrophic transport estimate for the Florida Current from the oxygen isotope composition of benthic foraminifera, *Paleoceanography*, *14*, 3, 360 – 373.

Lynch-Stieglitz, J., M.W. Schmidt, and W.B. Curry, 2011, Evidence from the Florida Straits for Younger Dryas ocean circulation changes, *Paleoceanography*, *26*, PA1205.

MacAyeal, D.R., 1993a, A Low-Order Model of the Heinrich Event Cycle, *Paleoceanography*, *8*, 6, 767 – 773.

MacAyeal, D.R., 1993b, Binge/Purge Oscillations of the Laurentide Ice Sheet as a Cause of the North Atlantic's Heinrich Events, *Paleoceanography*, *8*, 6, 775 – 784.

Martin, J.-M., and M. Meybeck, 1979, Elemental mass-balance of material carried by major world rivers, *Marine Chemistry*, *7*, 173 – 206.

Mashiotta, T. D., D.W. Lea, and H.J. Spero, 1999, Glacial-interglacial changes in Subantarctic sea surface temperature and $\delta^{18}O$-water using foraminiferal Mg, *Earth and Planetary Science Letters*, *170*, 417 – 432.

Maslin, M.A., and S.J. Burns, 2000, Reconstruction of the Amazon Basin Effective Moisture Availability over the Past 14,000 Years, *Science*, *290*, 2285 – 2287.

Mathien-Blard, E., and F. Bassinot, 2009, Salinity bias on the foraminifera Mg/Ca thermometry: Correction procedue and implications for past ocean hydrographic reconstructions, *Geochemistry Geophysics Geosystems*, 2008GC002353.

McCorkle, D.C., P.A. Martin, D.W. Lea, and G.P. Klinkhammer, 1995, Evidence of a dissolution effect on benthic foraminiferal shell chemistry: $\delta^{13}C$, Cd/Ca, Ba/Ca, and Sr/Ca results from the Ontong Java Plateau, *Paleoceanography*, *10*, 4, 699 – 714.

McManus, J.F., R. Francois, J.-M. Gherardi, L.D. Keigwin, and S. Brown-Leger, 2004, Collapse and rapid resumption of Atlantic meridional circulation linked to deglacial climate changes, *Nature*, *428*, 834 – 837.

Mertens, K.N., C. González, I. Delusina, and S. Louwye, 2009, 30 000 years of productivity and salinity variations in the late Quaternary Cariaco Basin revealed by dinoflagellate cysts, *Boreas*, *38*, 647 – 662.

Moore, W.S., 1999, The subterranean estuary: a reaction zone of ground water and sea water, *Marine Chemistry*, *65*, 111 – 125.

Moore, W. S., and T.J. Shaw, 1998, Chemical signals from submarine fluid advection onto the continental shelf, *Journal of Geophysical Research*, *103*, C10, 21,543 – 21,552.

Murphy, S. J., H. E. Hurlburt, and J. J. O'Brien, 1999, The connectivity of eddy variability in the Caribbean Sea, the Gulf of Mexico, and the Atlantic Ocean, *Journal of Geophysical Research*, *104*, 1431 – 1453.

NGRIP Members, 2004, High-resolution record of Northern Hemisphere climate extending into the last interglacial period, *Nature*, *431*, 147 – 151.

Nürnberg, D., J. Bijma, and C. Hemleben, 1996a, Assessing the reliability of magnesium in foraminiferal calcite as a proxy for water mass temperatures, *Geochimica et Cosmochimica Acta*, *60*, 5, 803 – 814.

Nürnberg, D., A. Müller, and R.R. Schneider, 2000, Paleo-sea surface temperature calculations in the equatorial east Atlantic from Mg/Ca ratios in planktic

foraminifera: A comparison to sea surface temperature estimates from $U_{37}^{K'}$, oxygen isotopes, and foraminiferal transfer function, *Paleoceanography*, *15*, 1, 124 – 134.

Oppo, D.W., Y. Rosenthal, and B.K. Linsley, 2009, 2,000-year-long temperature and hydrology reconstructions from the Indo-Pacific warm pool, *Nature*, *460*, 1113 – 1116.

Ortiz, J.D., A.C. Mix, and R.W. Collier, 1995, Environmental control of living symbiotic and asymbiotic foraminifera of the California Current, *Paleoceanography*, *10*, 6, 987 – 1009.

Ortner, P.B., T.N. Lee, P.J. Milne, R.G. Zika, M.E. Clarke, G.P. Podestá, P.K. Swart, P.A. Tester, L.P. Atkinson, and W.R. Johnson, 1995, Mississippi River flood waters that reached the Gulf Stream, *Journal of Geophysical Research*, *100*, C7, 13,595 – 13,601.

Otto-Bliesner, B. L., and E.C. Brady, 2010, The sensitivity of the climate response to the magnitude and location of freshwater forcing: last glacial maximum experiments, *Quaternary Science Reviews* , *29*, 56 – 73.

Peterson, L.C., G.H. Haug, K.A. Hughen, and U. Röhl, 2000, Rapid changes in the hydrologic cycle of the tropical Atlantic during the Last Glacial, *Science*, *290*, 1947 – 1951.

Peterson, L.C., and G.H. Haug, 2006, Variability in the mean latitude of the Atlantic Intertropical Convergence Zone as recorded by riverine input of sediments to the Cariaco Basin (Venezuela), *Paleogeography, Paleoclimatology, Paleoecology*, *234*, 97 – 113.

Piotrowski, A.M., S.L. Goldstein, S.R. Hemming, and R.G. Fairbanks, 2005, Temporal relationships of carbon cycling and ocean circulation at glacial boundaries, *Science*, *307*, 1933 – 1938.

Praetorius, S.K., J.F. McManus, D.W. Oppo, and W.B. Curry, 2008, Episodic reductions in bottom-water currents since the last ice age, *Nature*, *1*, 449 – 452.

Rahmstorf, S., 2002, Ocean circulation and climate during the past 120,000 years, *Nature*, *419*, 207 – 214.

Rasmussen, T.L., and E. Thomsen, 2012, Changes in planktic foraminiferal faunas, temperature and salinity in the Gulf Strean during the last 30,000 years: influence of meltwater via the Mississippi River, *Quaternary Science Reviews*, *33*, 42 – 54.

Romanova, V., G. Lohmann, K. Grosfeld, and M. Butzin, 2006, The relative role of oceanic heat transport and orography on glacial climate, *Quaternary Science Reviews*, *25*, 832 – 845.

Rosenthal, Y., G.P. Lohmann, K.C. Lohmann, and R.M. Sherrell, 2000, Incorporation and preservation of Mg in *Globigerinoides sacculifer*: Implications for reconstructing the temperature and $^{18}O/^{16}O$ of seawater, *Paleoceanography*, *15*, 1, 135 – 145.

Rosenthal, Y, and others, 2004, Interlaboratory comparison study of Mg/Ca and Sr/Ca measurements in planktonic foraminifera for paleoceanographic research, *Geochemistry Geophysics Geosystems*, *5*, 4, 2003GC000650.

Ruddiman, W.F., 1971, Pleistocene Sedimentation in the Equatorial Atlantic: Stratigraphy and Faunal Paleoclimatology, *Geological Society of America Bulletin*, *82*, 2, 283 – 302.

Sachs, J.P., and S.J. Lehman, 1999, Subtropical North Atlantic Temperatures 60,000 to 30,000 Years Ago, *Science*, *286*, 756 – 759.

Schmidt, G.A., G.R. Bigg, and E.J. Rohling, 1999, Global Seawater Oxygen-18 Database, http:// data.giss.nasa.gov/o18data/, GSFC Earth Sci. (GES) DAAC, Greenbelt, Md.

Schmidt, M.W., H.J. Spero, and D.W. Lea, 2004, Links between salinity variation in the Caribbean and North Atlantic thermohaline circulation, *Nature*, *428*, 160 – 163.

Schmidt, M.W., M.J. Vautravers, and H.J. Spero, 2006, Rapid subtropical North Atlantic salinity oscillations across Dansgaard-Oeschger cycles, *Nature*, *443*, 561 – 564.

Schmidt, M.W., and J. Lynch-Stieglitz, 2011, Florida Straits deglacial temperature and salinity change: Implications for tropical hydrologic cycle variability during the Younger Dryas, *Paleoceanography*, *26*, PA4205.

Schmidt, M.W., W.A. Weinlein, F. Marcantonio, and J. Lynch-Stieglitz, *in press*, Solar forcing of Florida Straits surface salinity during the early Holocene, *Paleoceanography*.

Schmitz, W.J. Jr., and M.S. McCartney, 1993, On the North Atlantic Circulation. *Reviews of Geophysics*, *31*, 1, 29 – 49.

Schmitz, W.J., and P.L. Richardson, 1991, On the sources of the Florida Current, *Deep Sea Research*, *Part A*, *38*, 379 – 409.

Schmuker, B., and R. Schiebel, 2002, Planktic foraminifers and hydrography of the eastern and northern Caribbean Sea, *Marine Micropaleontology*, *46*, 387 – 403.

Schrag, D.P., G. Hampt, and D.W. Murray, 1996, Pore Fluid Constraints on the Temperature and Oxygen Isotopic Composition of the Glacial Ocean, *Science*, *272*, 1930 – 1932.

Schrag, D.P., J.F. Adkins, K. McIntyre, J.L. Alexander, D.A. Hodell, C.D. Charles, and J.F. McManus, 2002, The oxygen isotopic composition of seawater during the Last Glacial Maximum, *Quaternary Science Reviews*, *21*, 331 – 342.

Seager, R., D.S. Battisti, J. Yin, N. Gordon, N. Naik, A.C. Clement, and M.A. Cane, 2002, Is the Gulf Stream responsible for Europe's mild winters? *Quarterly Journal of the Royal Meteorlogical Society*, *128*, 2563 – 2586.

Shackleton, N.J., and N.D. Opdyke, 1973, Oxygen Isotope and Palaeomagnetic Stratrigraphy of Equatorial Pacific Core V28-238: Oxygen Isotope Temperatures and Ice Volumes on a 10^5 Year and 10^6 Year Scale, *Quaternary Research*, *3*, 39 – 55.

Shackleton, N.J., J. Imbrie, and M.A. Hall, 1983, Oxygen and carbon isotope record of East Pacific core V19-30: implications for the formation of deep water in the late Pleistocene North Atlantic, *Earth and Planetary Science Letters*, *65*, 233 – 244.

Siddall, M., E.J. Rohling, A. Almogi-Labin, C. Hemleben, D. Meischner, I. Schmelzer, and D.A. Smeed, 2003, Sea-level fluctuations during the last glacial cycle, *Nature*, *423*, 853 – 858.

Stouffer, R. J., J. Yin, J.M. Gregory, K.W. Dixon, M.J. Spelman, W. Hurlin, A.J. Weaver, M. Eby, G.M. Flato, H. Hasumi, A. Hu, J.H. Jungclaus, I.V. Kamenkovich, A. Levermann, M. Montoya, S. Murakami, S. Nawrath, A. Oka, W.R. Peltier, D.Y. Robitaille, A. Sokolov, G. Vettoretti, and S.L. Weber, 2006, Investigating the causes of the response of thermohaline circulation to past and future climate change, *Journal of Climate*, *19*, 1365 – 1387.

Urey, H.C., 1947, The thermodynamic properties of isotopic substances, *Journal of the Chemical Society*, 562 – 581.

Vautravers, M.J., N.J. Shackleton, C. Lopez-Martinez, and J.O. Grimalt, 2004, Gulf Stream variability during marine isotope stage 3, *Paleoceanography*, *19*, PA2011.

Vellinga, M., and R. Wood, 2002, Global climatic impacts of a collapse of the Atlantic thermohaline circulation. *Climatic Change*, *54*, 251 – 267.

Voelker, A.H.L., and workshop participants, 2002, Global distribution of centennial-scale records for Marine Isotope Stage (MIS) 3: a database, *Quaternary Science Reviews*, *21*, 1185 – 1212.

Von Damm, K.L., J.M. Edmond, B. Grant, C.I. Measures, B. Walden, and R.F. Weiss, 1985, Chemistry of submarine hydrothermal solutions at 21°N, East Pacific Rise, *Geochimica et Cosmochimica Acta*, *49*, 2197 – 2220.

Waelbroeck, C., L. Labeyrie, E. Michel, J.C. Duplessy, J.F. McManus, K. Lambeck, E. Balbon, and M. Labracherie, 2002, Sea-level and deep water temperature changes derived from benthic foraminifera isotopic changes, *Quaternary Science Reviews*, *21*, 295 – 305.

Wan, X., P. Chang, R. Saravanan, R. Zhang, and M.W. Schmidt, 2009, On the interpretation of Caribbean paleo-temperature reconstructions during the Younger Dryas, *Geophysical Research Letters*, *36*, L02701.

Wang, Y.J., H. Cheng, R.L. Edwards, Z.S. An, J.Y. Wu, C.-C. Shen, and J.A. Dorale, 2001, A high-resolution absolute-dated Late Pleistocene monsoon record from Hulu Cave, China, *Science*, *294*, 2345 – 2348.

Wang, X., A.S. Auler, R.L. Edwards, H. Cheng, E. Ito, Y. Wang, X. Kong, and M. Solheid, 2007, Millennial-scale precipitation changes in southern Brazil over the past 90,000 years, *Geophysical Research Letters*, *34*, L23701.

Weldeab, S., R.R. Schneider, and M. Kölling, 2006, Deglacial sea surface temperature and salinity increase in the western tropical Atlantic in synchrony with high latitude climate instabilities, *Earth and Planetary Science Letters*, *241*, 699 – 706.

Weldeab, S., D.W. Lea, R.R. Schneider, and N. Andersen, 2007, 155,000 years of West African monsoon and ocean thermal evolution, *Science*, *316*, 1303 – 1307.

Wunsch, C., 2006, Abrupt climate change: An alternate view, *Quaternary Research*, *65*, 191 – 203.

Yokoyama, Y., K. Lambeck, P. De Deckker, P. Johnston, and L.K. Fifield, 2000, Timing of the Last Glacial Maximum from observed sea-level minima, *Nature*, *406*, 713 – 716.

Zhang, R., and T.L. Delworth, 2005, Simulated tropical response to a substantial weakening of the Atlantic thermohaline circulation, *Journal of Climate*, *18*, 1853 – 1860.

APPENDIX A

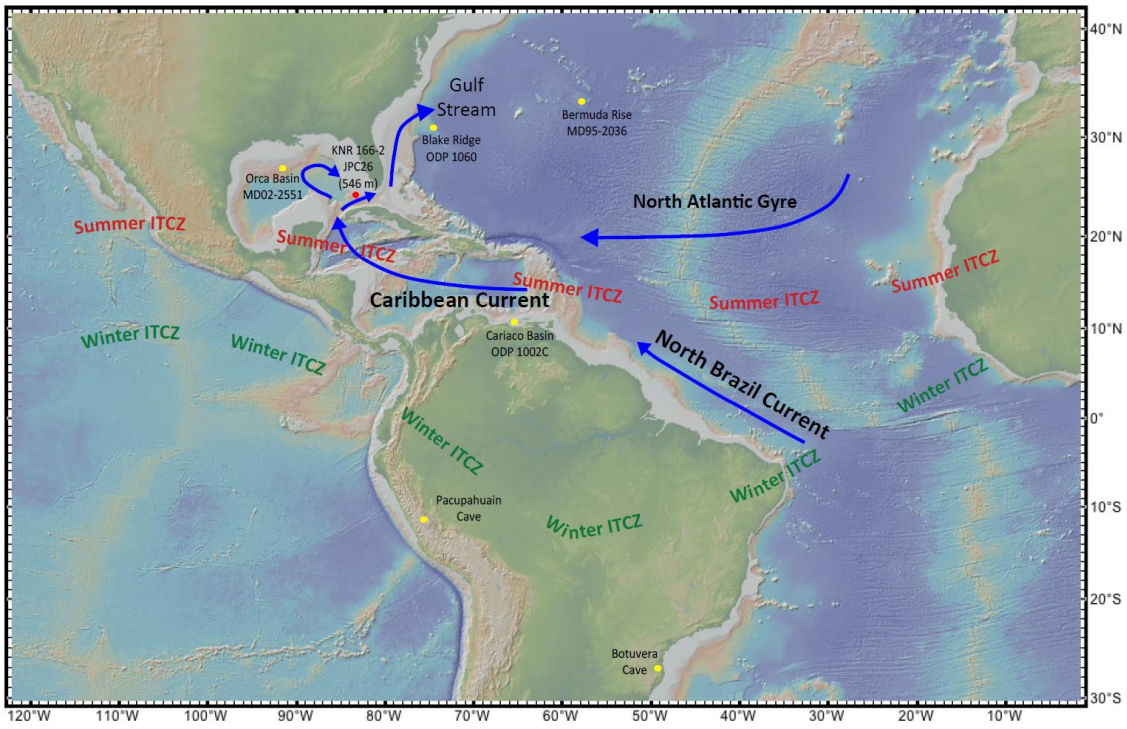

Figure 1 Study Area. The location of the core used in this study (red circle), KNR166-2 JPC26 on the northern margin of the Florida Straits. Also noted are the positions of the Orca Basin in the northern Gulf of Mexico, the Blake Ridge and Bermuda Rise in the North Atlantic, the Cariaco Basin in the western tropical Atlantic, and Pacupahuain and Botuverá caves from South America (yellow circles) (map generated using GeoMapApp).

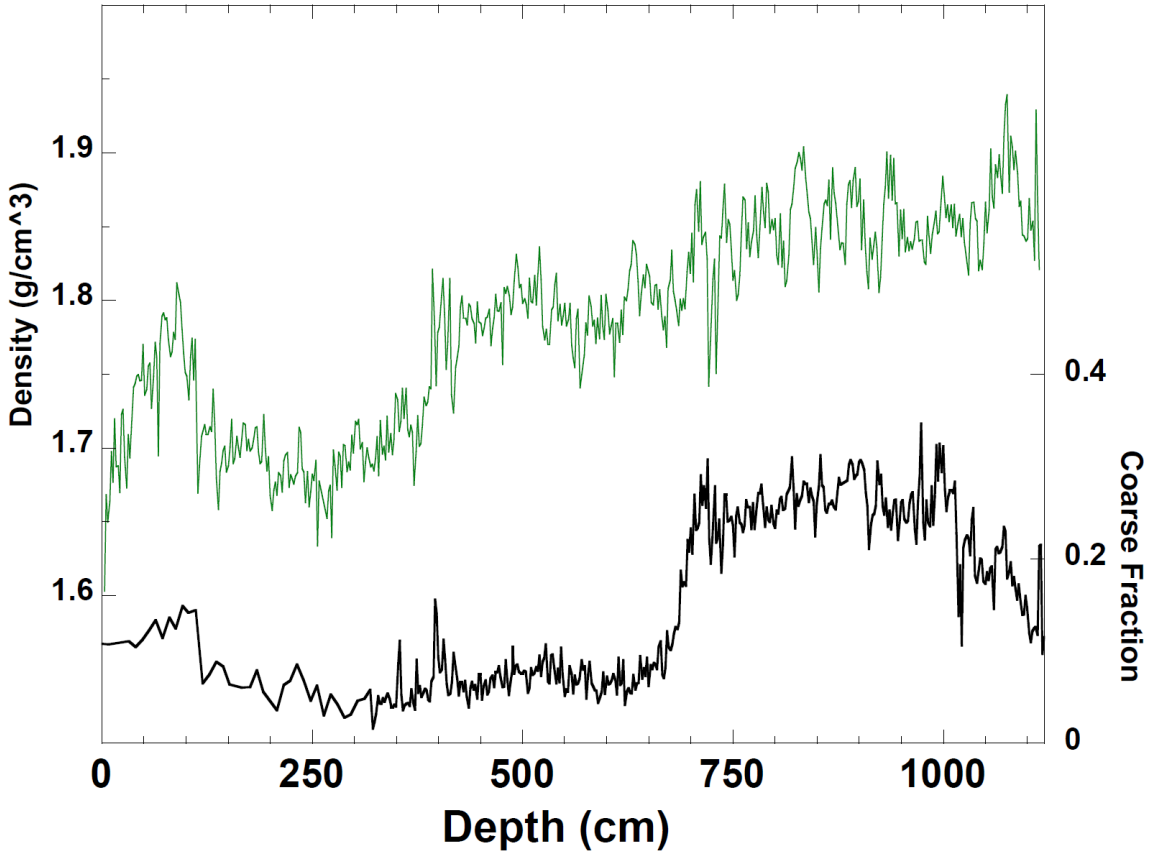

Figure 2 Sedimentological Properties. (A) Density (g/cm^3) and (B) coarse fraction in JPC26.

A.

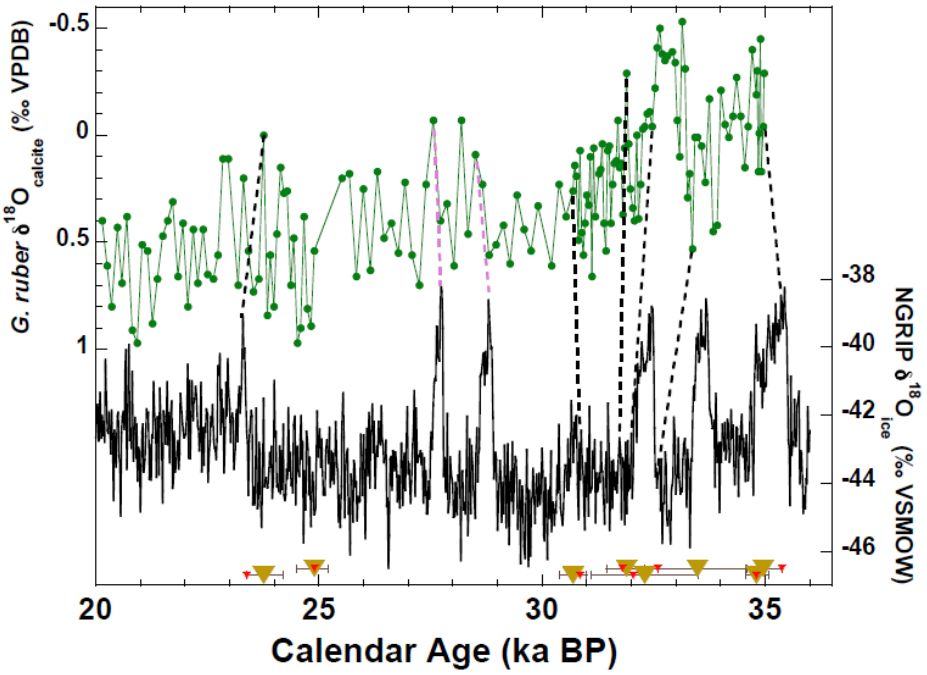
G. ruber δ18Ocalcite (‰ VPDB)
-0.5
0
0.5
1
NGRIP δ18Oice (‰ VSMOW)
-38
-40
-42
-44
-46
20
25
30
35
Calendar Age (ka BP)

B.

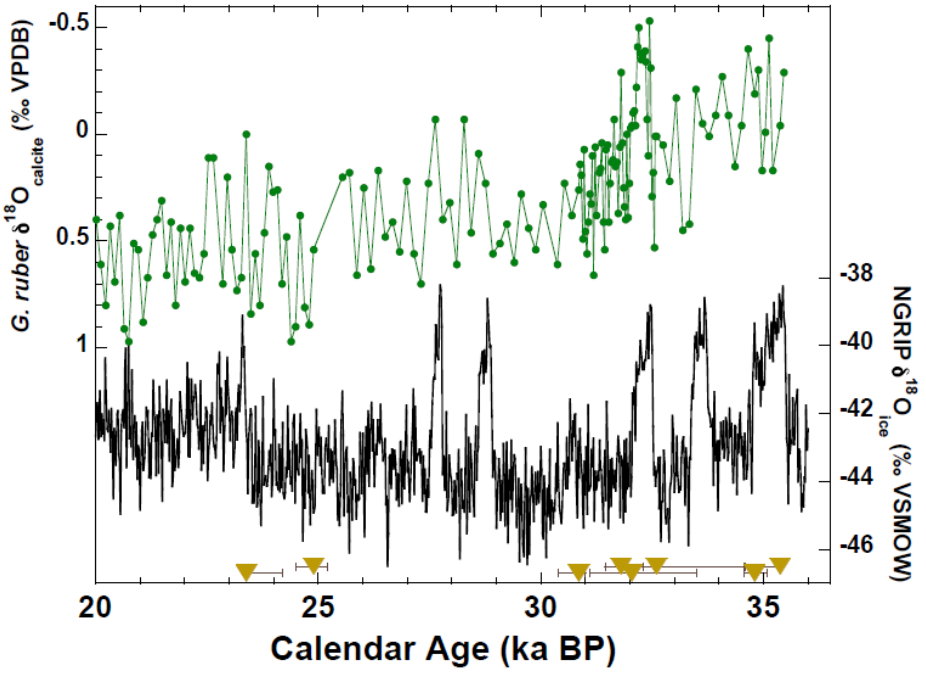
G. ruber δ18Ocalcite (‰ VPDB)
-0.5
0
0.5
1
NGRIP δ18Oice (‰ VSMOW)
-38
-40
-42
-44
-46
20
25
30
35
Calendar Age (ka BP)

Figure 3 Age Model. (A) Most probable calendar ages for JPC26 based on ^{14}C dates from mixed samples of *G. ruber* and *G. sacculifer* shell material and (B) tuned calendar ages for JPC26. Radiocarbon years were calibrated to calendar years using CALIB 6.0 [*Stuiver et al.,* 2011] and a standard marine reservoir age correction of 400 years [*Hughen et al.*, 2004]. Gold triangles on the x-axis indicate intervals with radiocarbon dates and their associated error. Red triangles on the x-axis in figure A indicate new tuned values. Dashed black lines in figure A indicate where $\delta^{18}O_C$ values were tuned to NGRIP $\delta^{18}O_{ICE}$ record using intervals where radiocarbon ages were measured. Dashed purple lines indicate points where $\delta^{18}O_C$ values were tuned to NGRIP $\delta^{18}O_{ICE}$ record.

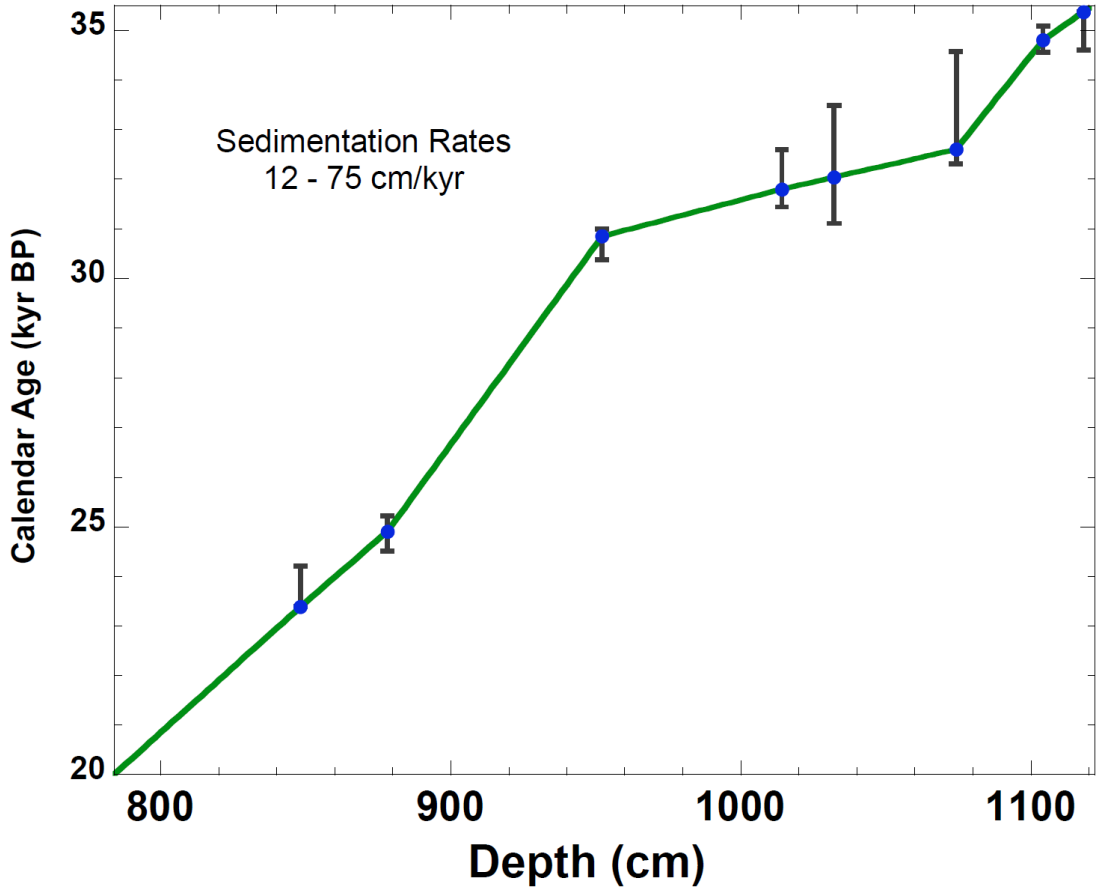

Figure 4 Sedimentation Rates. Calendar age vs. core depth for JPC26 based on ^{14}C dates from mixed samples of *G. ruber* and *G. sacculifer* shell material. Radiocarbon years were calibrated to calendar years using CALIB 6.0 [*Stuiver et al.*, 2011] and a standard marine reservoir age correction of 400 years [*Hughen et al.*, 2004].

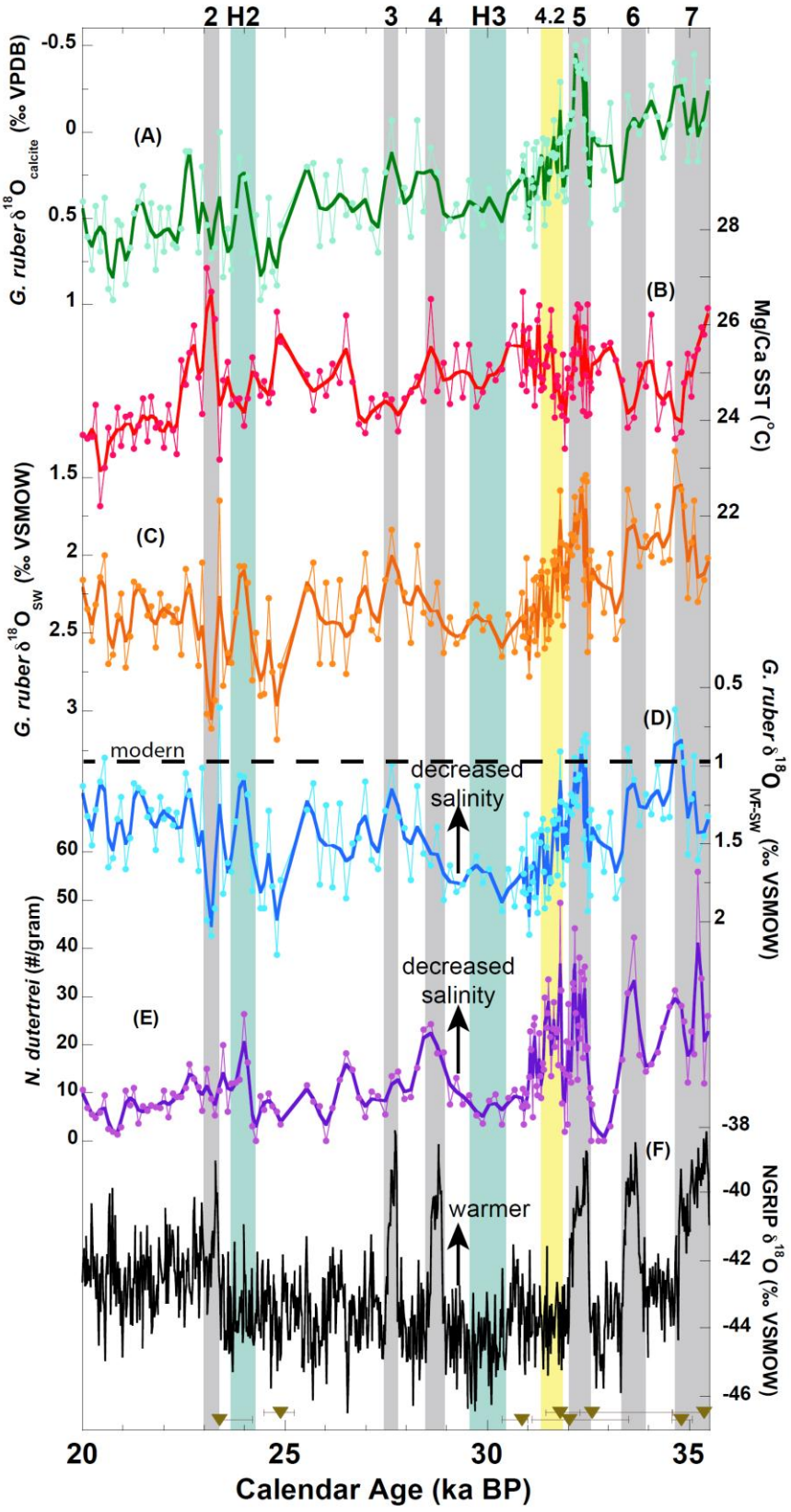
2
H2
3
4
H3
4.2
5
6
7
(A)
(B)
(C)
(D)
(E)
(F)
modern
decreased salinity
decreased salinity
warmer
G. ruber δ18Ocalcite (‰ VPDB)
Mg/Ca SST (°C)
G. ruber δ18Osw (‰ VSMOW)
G. ruber δ18OIVF-SW (‰ VSMOW)
N. dutertrei (#/gram)
NGRIP δ18O (‰ VSMOW)
Calendar Age (ka BP)

Figure 5 *G. ruber* $\delta^{18}O_C$, Mg/Ca-SST, $\delta^{18}O_{SW}$, $\delta^{18}O_{IVF-SW}$, *N. dutertrei abundances*, and NGRIP $\delta^{18}O_{ICE}$. **(A)** $\delta^{18}O_C$ values in *G. ruber* collected from the Florida Straits (JPC26) (green circles with weighted 3-point smooth) and corresponding unsmoothed values (light green line). **(B)** Mg/Ca-SSTs (red circles with weighted 3-point smooth) and corresponding actual SST values scale from JPC26 calculated using the general planktonic relationship from *Anand et al.* [2003]: Mg/Ca = 0.38 exp 0.09(SST). The optimistic 1σ error of ±0.5°C is shown. In blue along the SST axis are the high and low annual SST values for the Florida Straits and the average annual SST. **(C)** Calculated $\delta^{18}O_{SW}$ values (orange circles with weighted 3-point smooth) from the Florida Straits (JPC26). **(D)** Calculated $\delta^{18}O_{IVF-SW}$ values (blue circles with weighted 3-point smooth) from the Florida Straits (JPC26). **(E)** *Neogloboquadrina dutertrei* abundances (purple circles with weighted 3-point smooth) in Florida Straits (JPC26). **(F)** NGRIP $\delta^{18}O_{ICE}$ record. Gold triangles on the x-axis indicate intervals with radiocarbon dates and their associated error.

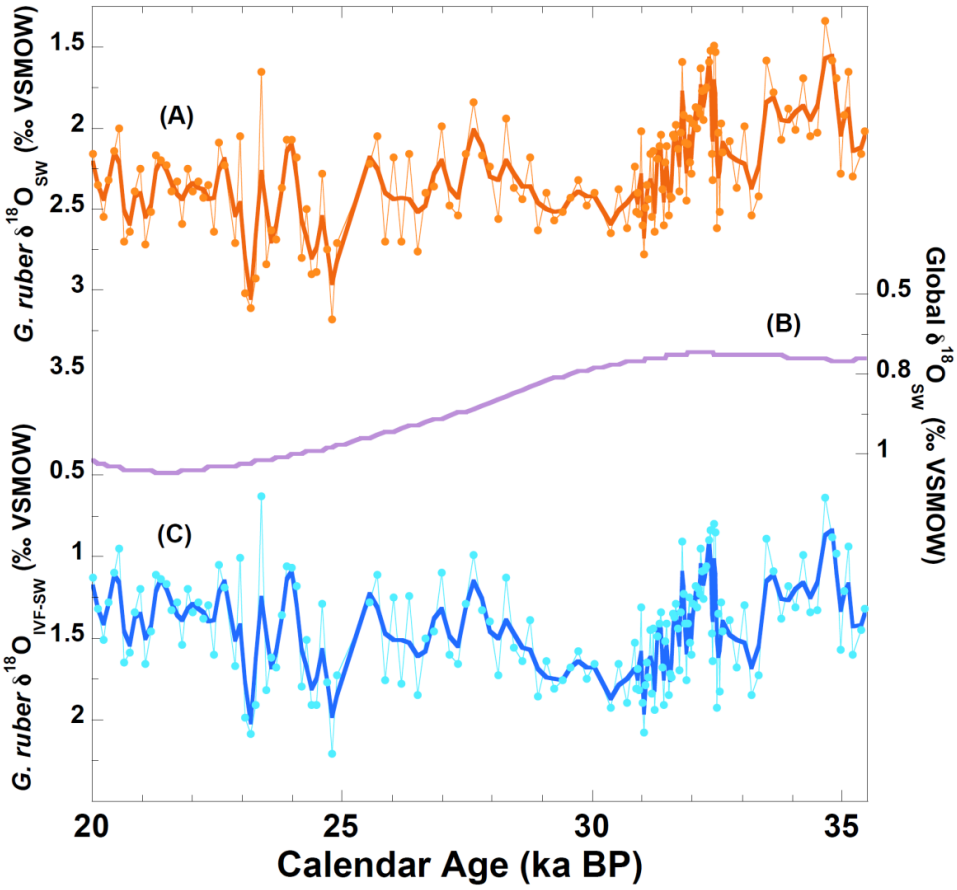

Figure 6 $\delta^{18}O_{SW}$ and $\delta^{18}O_{IVF\text{-}SW}$. (**A**) Calculated $\delta^{18}O_{SW}$ values from JPC26 (dark orange circles with weighted 3-point smooth) using the *Bemis et al.* [1998] relationship: $(T°C) = 16.5 - 4.80 (\delta^{18}O_{calcite} - \delta^{18}O_{SW})$ and the Mg/Ca-SST relationship from *Anand et al.* [2003]. (**B**) Global $\delta^{18}O_{SW}$ change due to continental ice volume variability (purple) from a compilation of sea level records for 20 – 35.45 ka BP [*Yokoyama et al.*, 2000; *Waelbroeck et al.*, 2002] and the relationship that a one meter increase in sea level change equates to a change of –0.00875‰ in global $\delta^{18}O_{sw}$ values [*Schrag et al.*, 2002]. (**C**) Calculated ice volume free $\delta^{18}O_{SW}$ ($\delta^{18}O_{IVF\text{-}SW}$) (blue circles with weighted 3-point smooth) calculated by correcting for global $\delta^{18}O_{SW}$ change due to continental ice volume variability.

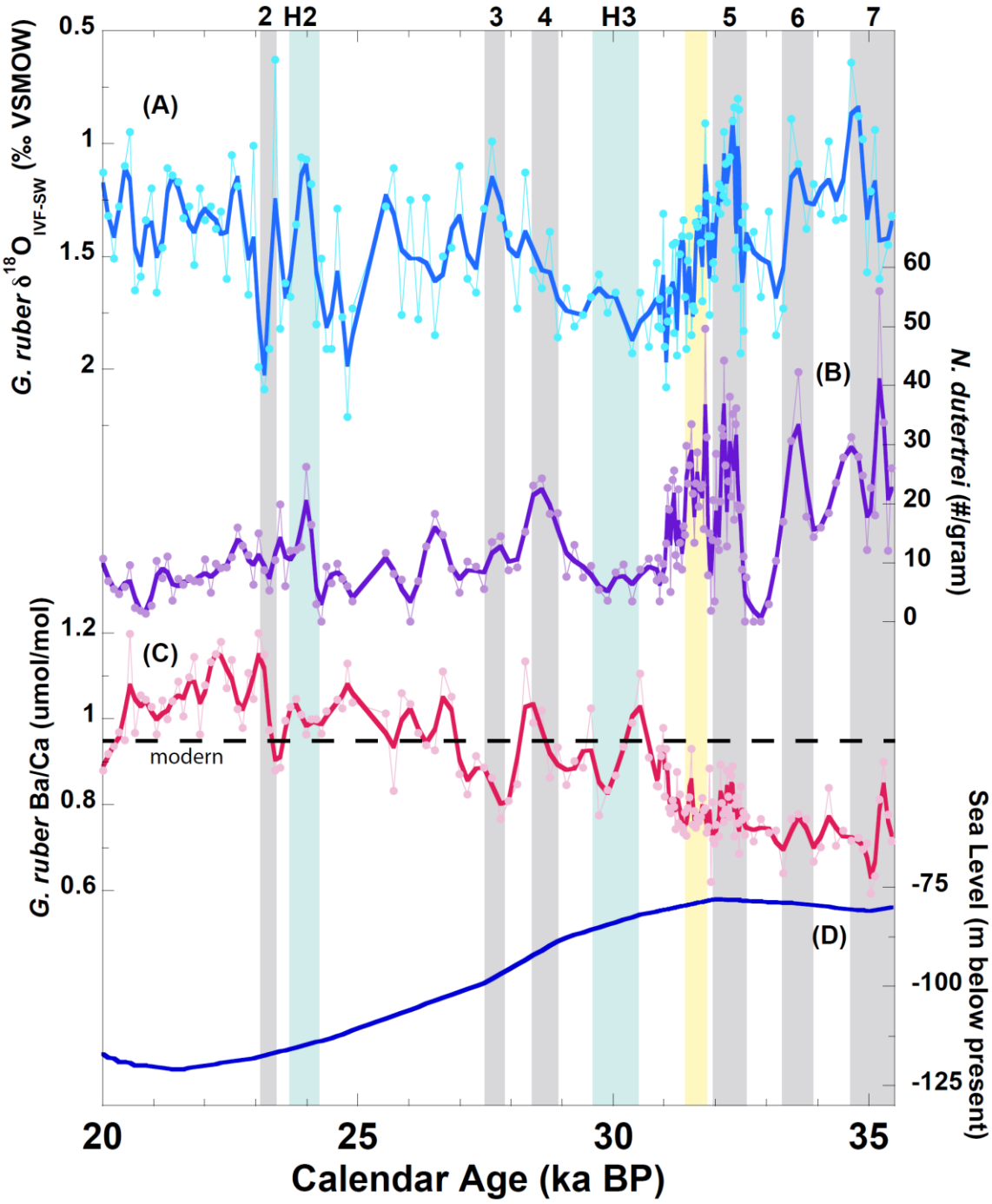
2 H2
3
4
H3
5
6
7
(A)
(B)
(C)
(D)
modern
G. ruber δ18OIVF-SW (‰ VSMOW)
N. dutertrei (#/gram)
G. ruber Ba/Ca (umol/mol)
Sea Level (m below present)
Calendar Age (ka BP)
0.5
1
1.5
2
60
50
40
30
20
10
0
1.2
1
0.8
0.6
-75
-100
-125
20
25
30
35

Figure 7 $\delta^{18}O_{IVF\text{-}SW}$, *N. dutertrei*, Ba/Ca, and Sea Level Comparison. (**A**) Calculated $\delta^{18}O_{IVF\text{-}SW}$ values (blue circles with weighted 3-point smooth) from JPC26 (**B**) *N. dutertrei* abundance record (purple circles with weighted 3-point smooth) in JPC26. (**C**) Foraminiferal Ba/Ca ratios in *G. ruber* (red circles with weighted 3-point smooth) from JPC26 (**D**) Sea level changes from 20 – 35.45 ka BP [*Yokoyama et al.*, 2000; *Waelbroeck et al.*, 2002].

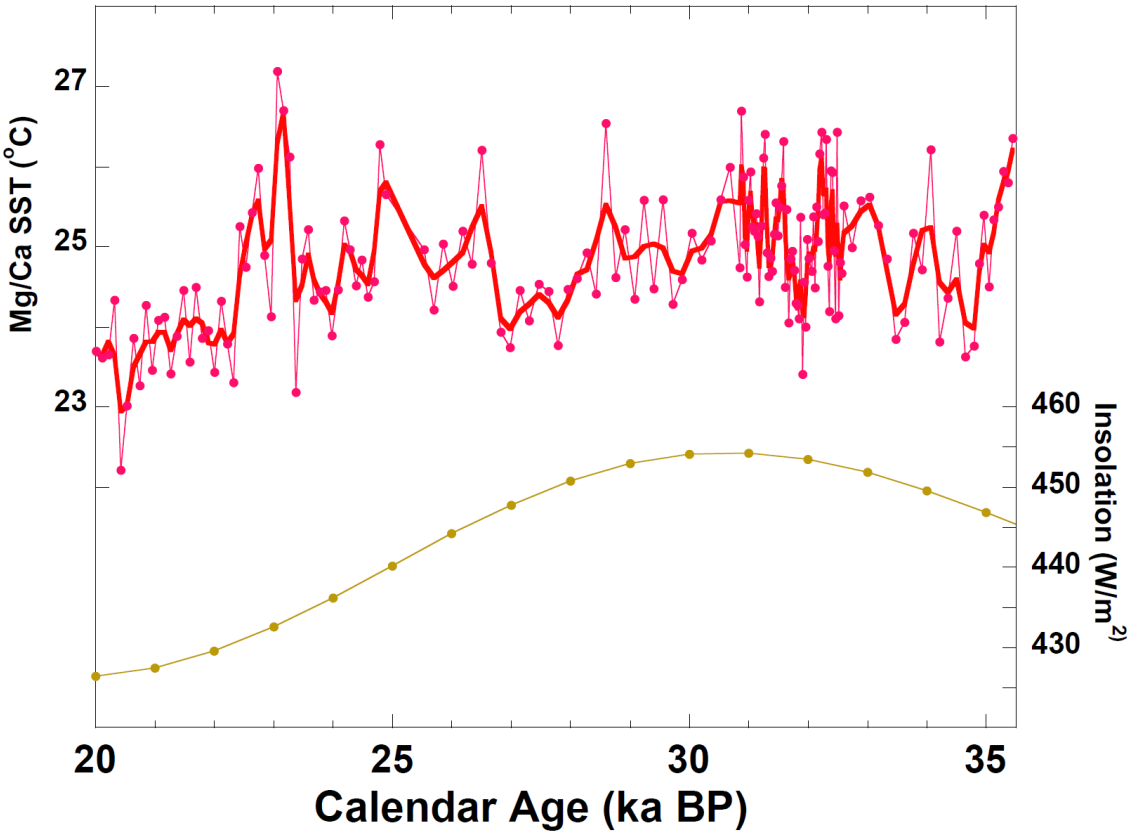

Figure 8 Mg/Ca-SST and Insolation Changes. (A) Mg/Ca-SST reconstructions calculated using the traditional relationship in *Anand et al*. [2003] (red circles with weighted 3-point smooth) and **(B)** insolation changes (yellow circles) at 10°N from 20 – 35.5 ka BP.

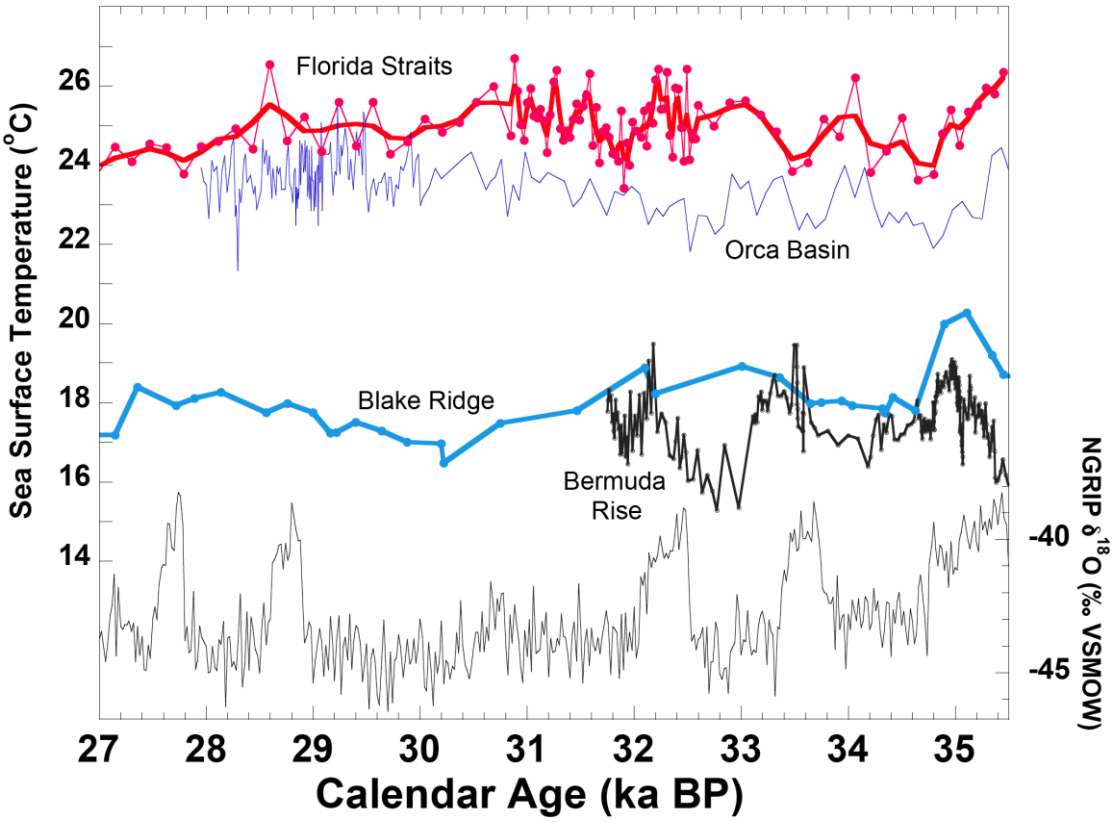

Figure 9 North Atlantic SST Comparison. A comparison between SST records from the Florida Straits [*this study*], Orca Basin [*Hill et al.*, 2006], Blake Ridge [*Vautravers et al.*, 2004] and Bermuda Rise [*Sachs and Lehman*, 1999] and the NGRIP $\delta^{18}O_{ICE}$ record.

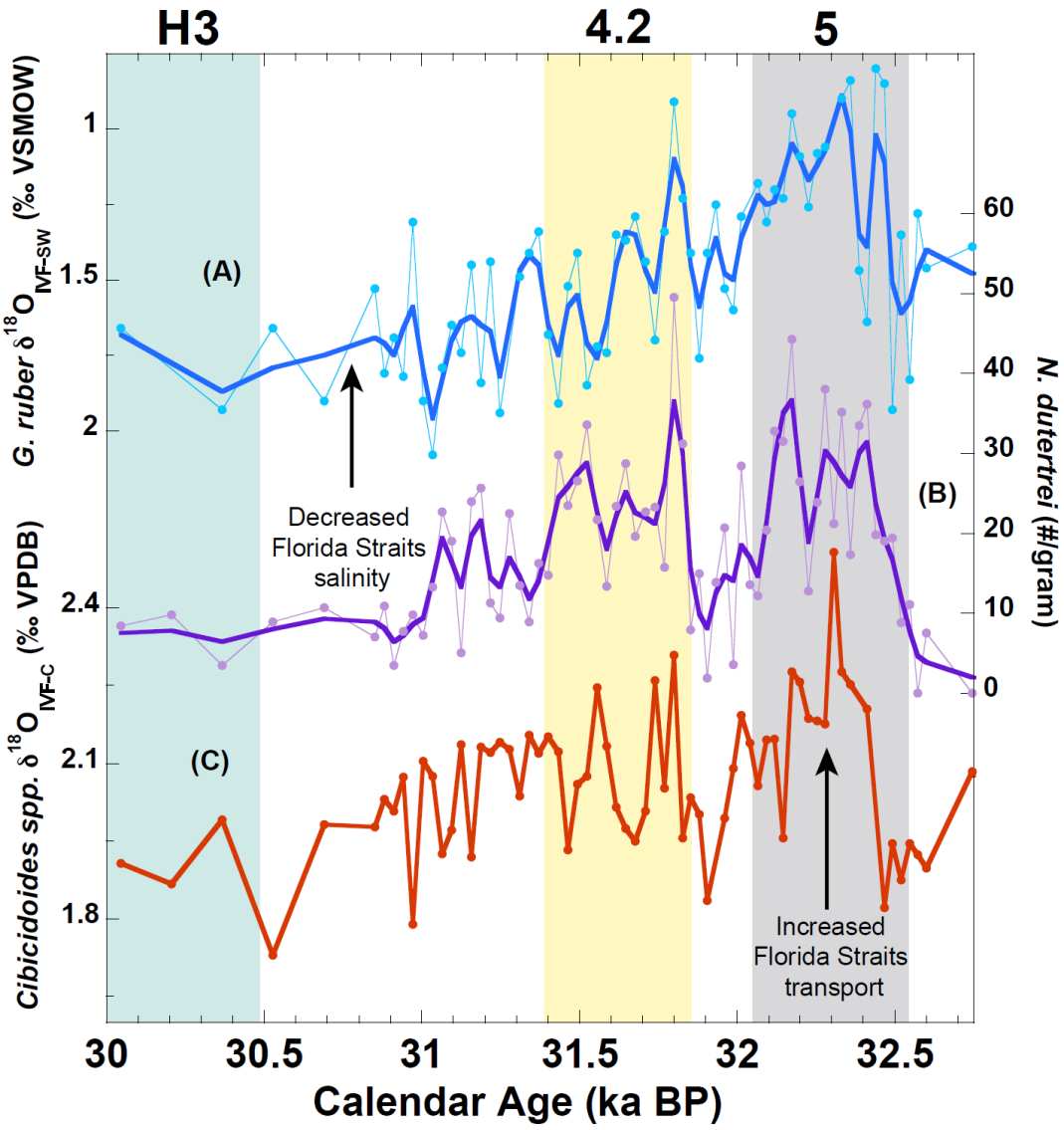
H3
4.2
5
G. ruber δ18OIVF-SW (‰ VSMOW)
Cibicidoides spp. δ18OIVF-C (‰ VPDB)
N. dutertrei (#/gram)
(A)
(B)
(C)
Decreased Florida Straits salinity
Increased Florida Straits transport
1
1.5
2
2.4
2.1
1.8
60
50
40
30
20
10
0
30
30.5
31
31.5
32
32.5
Calendar Age (ka BP)

Figure 10 Florida Straits Sea Surface Salinity and Florida Current Strength Comparison Across D-O 5. **(A)** $\delta^{18}O_{IVF\text{-}SW}$ (blue circles with weighted 3-point smooth) in JPC26. **(B)** *N. dutertrei* abundance record (purple circles with weighted 3-point smooth) in JPC26. **(C)** Benthic $\delta^{18}O_{IVF\text{-}C}$ record (orange circles) in JPC26 [*Lynch-Stieglitz et al.*, in prep]. Note the lead in *N. dutertrei*/gram over benthic $\delta^{18}O_{IVF\text{-}C}$ in gray shaded box (interstadial 5). Yellow shaded bar represents return to interstadial-like conditions in the tropics after interstadial 5.

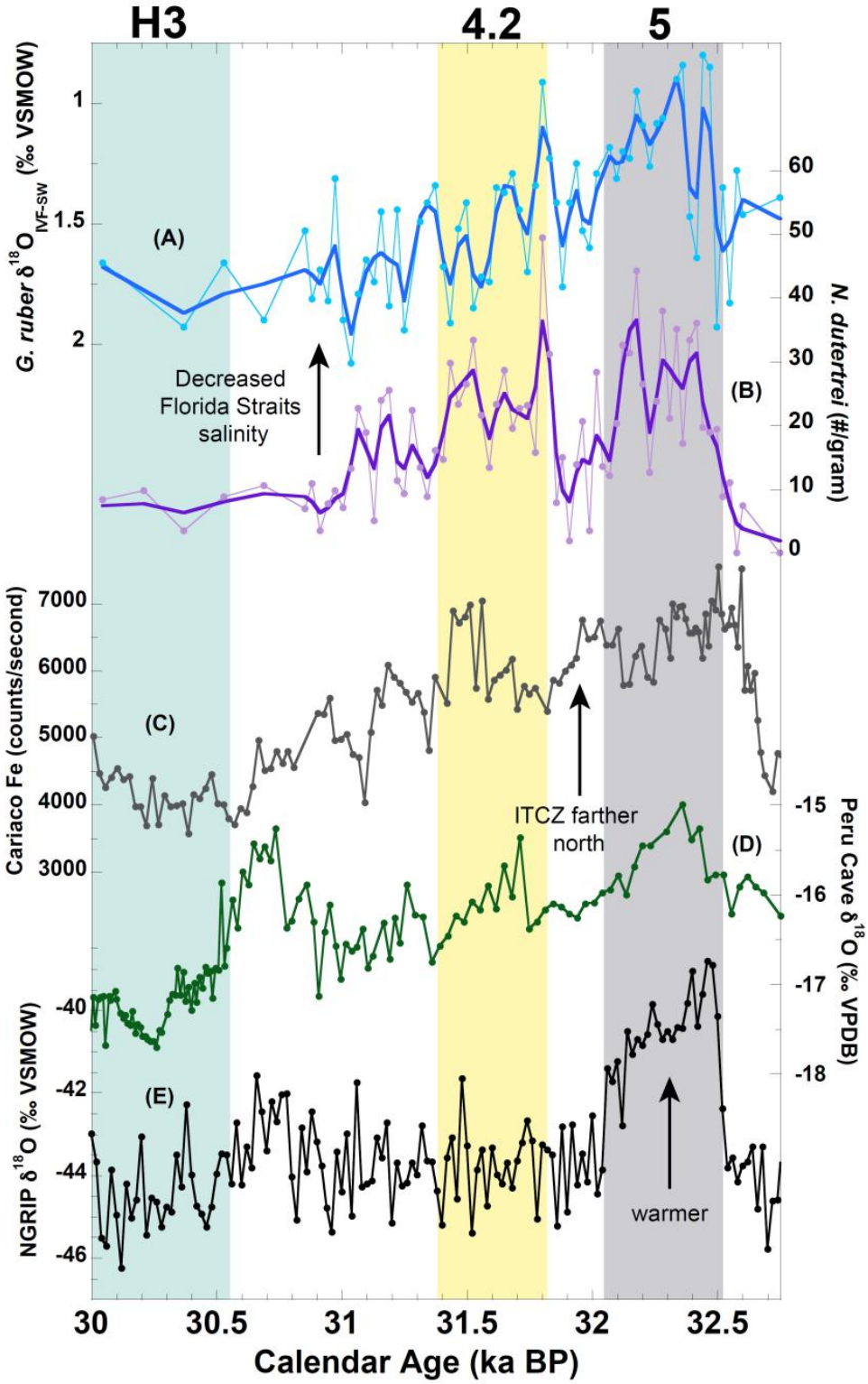
H3
4.2
5
G. ruber δ18O IVF-SW (‰ VSMOW)
1
1.5
2
(A)
Decreased
Florida Straits
salinity
(B)
N. dutertrei (#/gram)
60
50
40
30
20
10
0
Cariaco Fe (counts/second)
7000
6000
5000
4000
3000
(C)
ITCZ farther
north
(D)
Peru Cave δ18O (‰ VPDB)
-15
-16
-17
-18
NGRIP δ18O (‰ VSMOW)
-40
-42
-44
-46
(E)
warmer
30
30.5
31
31.5
32
32.5
Calendar Age (ka BP)

Figure 11 Tropical Hydrologic Cycle Comparison. **(A)** Calculated $\delta^{18}O_{IVF\text{-}SW}$ values (blue circles with weighted 3-point smooth) from the Florida Straits (JPC26). **(B)** *N. dutertrei* abundances in Florida Straits (JPC26) (blue circles with weighted 3-point smooth). **(C)** Cariaco Basin Fe record (gray circles) [*Peterson et al.*, 2000]. **(D)** Pacupahuain Cave speleothem $\delta^{18}O_C$ record (green circles) from Peru [*Kanner et al.*, 2012]. **(E)** NGRIP $\delta^{18}O_{ICE}$ record (black circles).

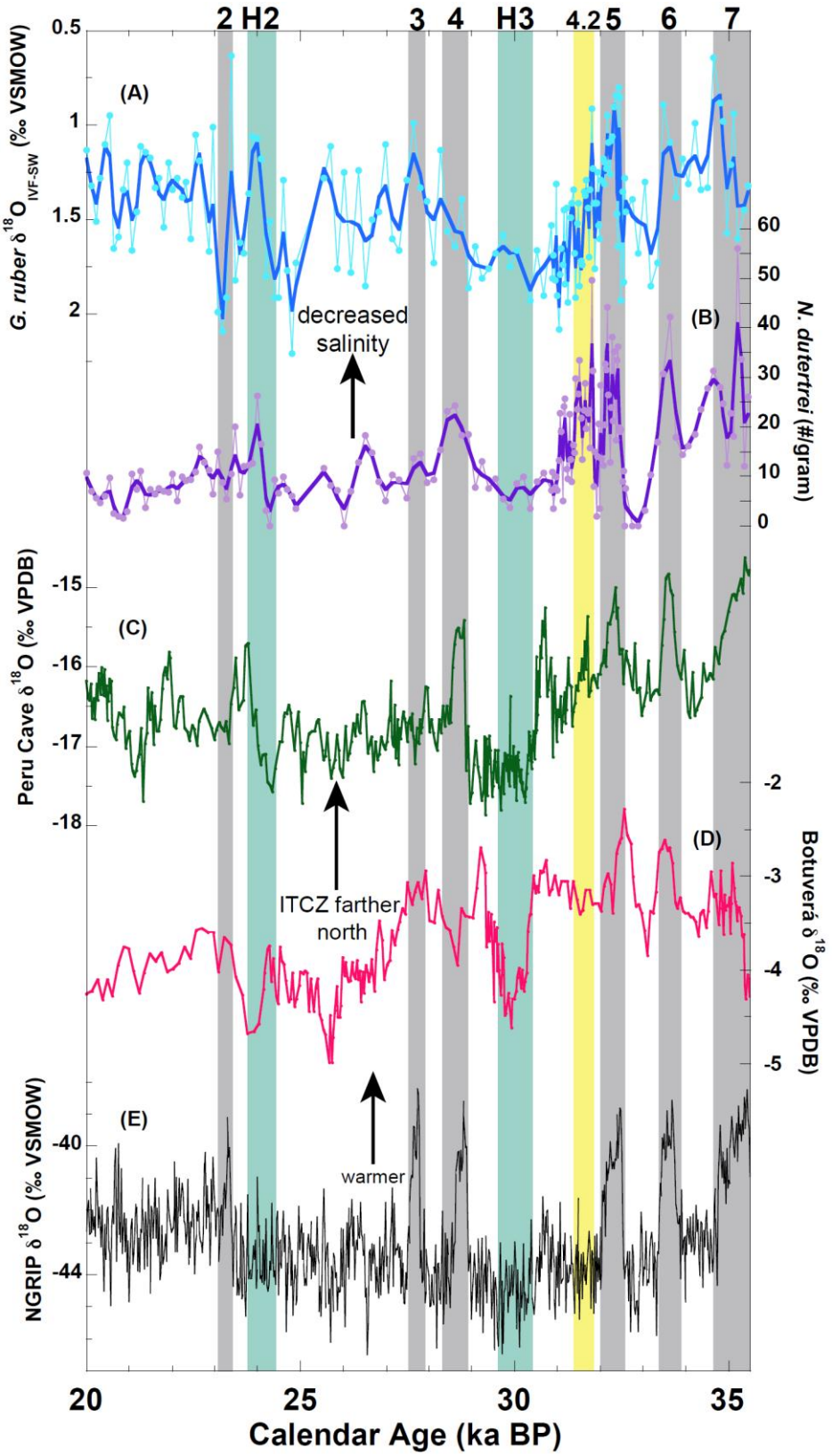
2
H2
3
4
H3
4.2
5
6
7
(A)
(B)
(C)
(D)
(E)
decreased salinity
ITCZ farther north
warmer
G. ruber δ18O IVF-SW (‰ VSMOW)
N. dutertrei (#/gram)
Peru Cave δ18O (‰ VPDB)
Botuverá δ18O (‰ VPDB)
NGRIP δ18O (‰ VSMOW)
0.5
1
1.5
2
60
50
40
30
20
10
0
-15
-16
-17
-18
-2
-3
-4
-5
-40
-44
20
25
30
35
Calendar Age (ka BP)

Figure 12 JPC26 Sea Surface Salinity and Speleothem Comparison. (A) Calculated $\delta^{18}O_{IVF\text{-}SW}$ values (blue circles with weighted 3-point smooth) from the Florida Straits (JPC26). **(B)** *N. dutertrei* abundances in Florida Straits (JPC26) (purple circles with weighted 3-point smooth). **(C)** Pacupahuain Cave speleothem $\delta^{18}O_C$ record (green circles with weighted 3-point smooth) from Peru [*Kanner et al.*, 2012] **(D)** Botuverá Cave $\delta^{18}O_C$ record (pink circles) from Brazil **(E)** NGRIP $\delta^{18}O_{ICE}$ record (black circles).

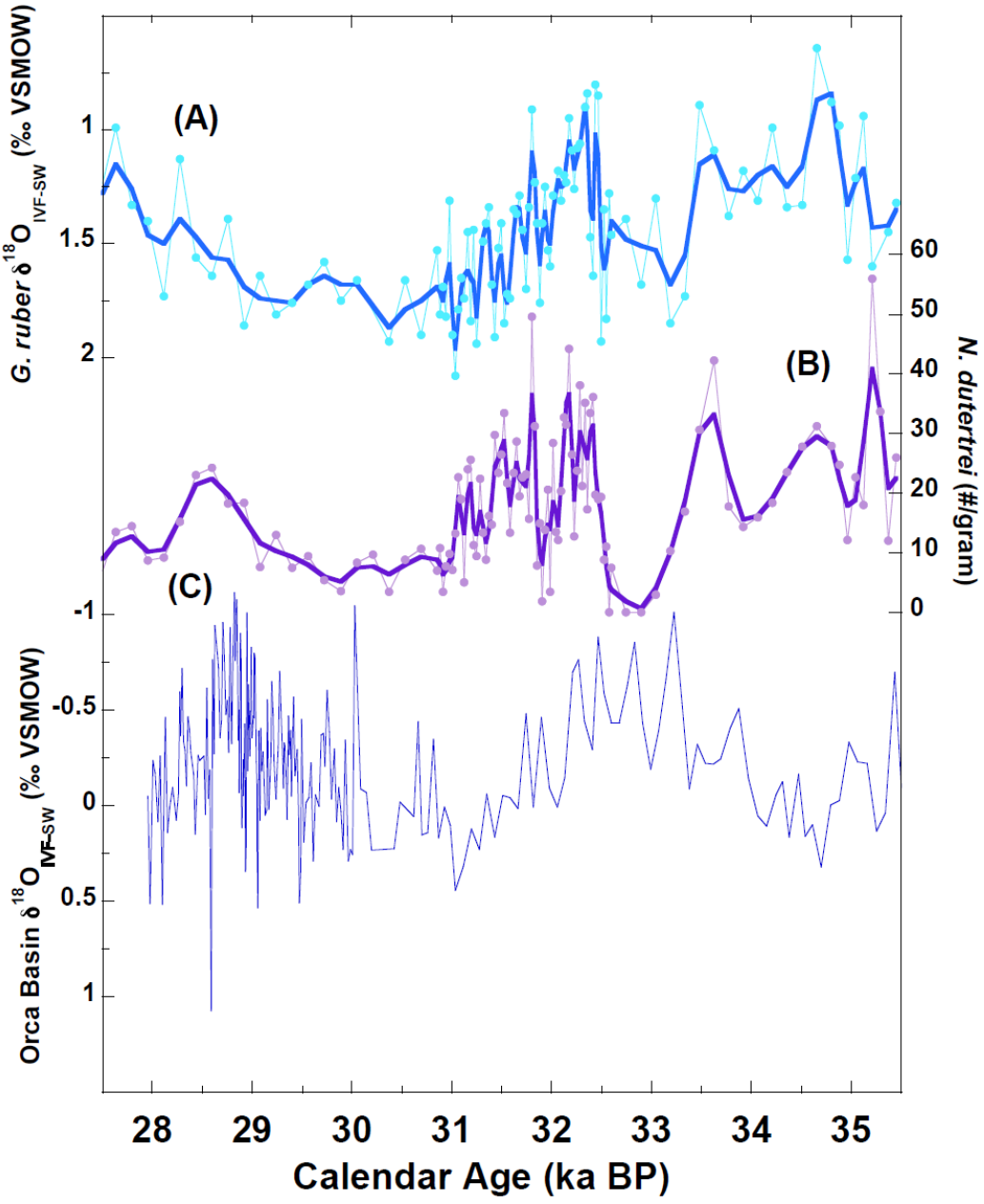

Figure 13 Florida Straits and Gulf of Mexico Surface Salinity Comparison. (A) Calculated $\delta^{18}O_{IVF\text{-}SW}$ values (blue circles with weighted 3-point smooth) from the Florida Straits (JPC26). **(B)** *N. dutertrei* abundances (purple circles with weighted 3-point smooth) in Florida Straits (JPC26). **(C)** Orca Basin $\delta^{18}O_{IVF\text{-}SW}$ values (blue line) [*Hill et al.*, 2006].

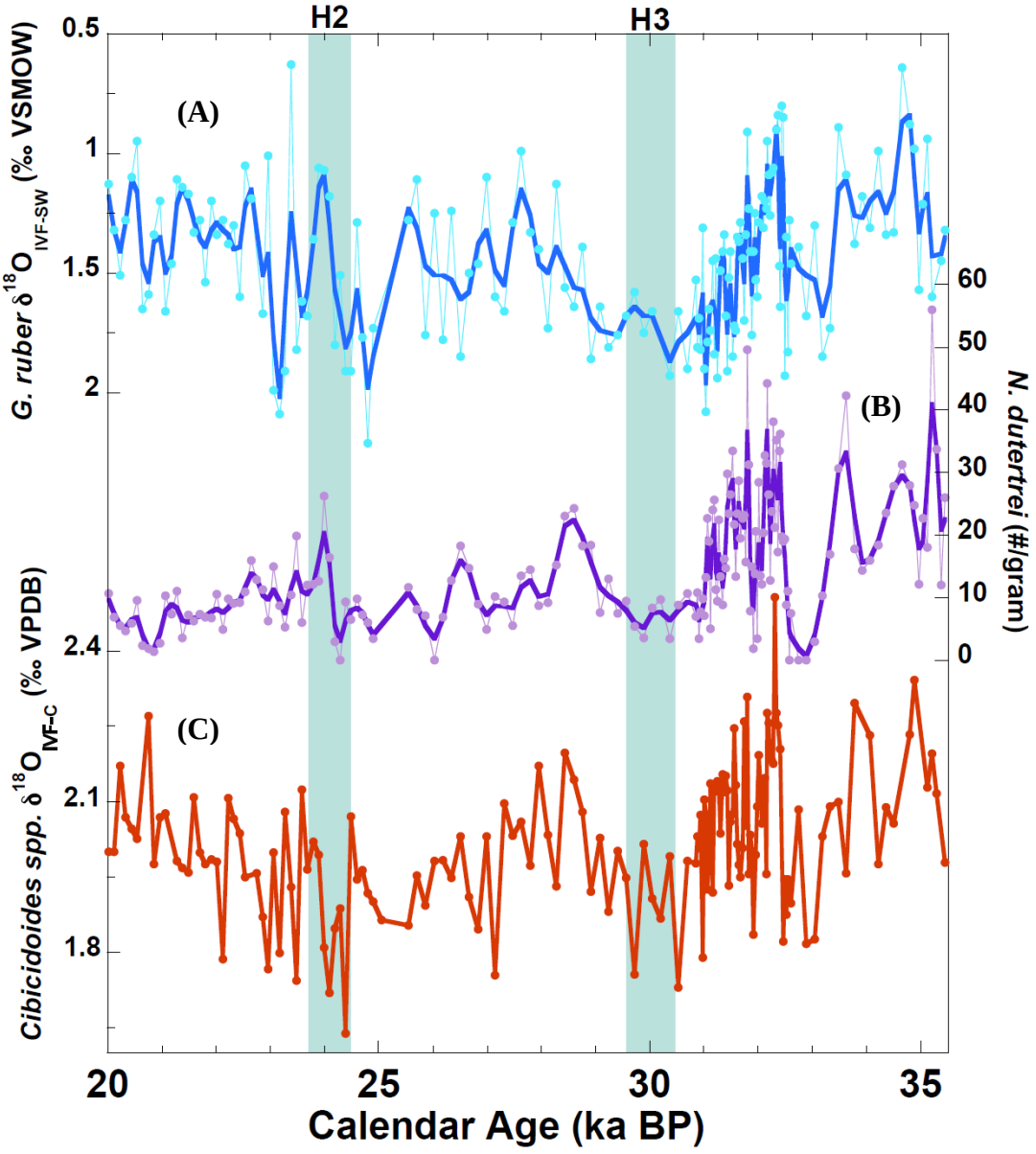

Figure 14 JPC26 Planktic and Benthic Comparison. **(A)** Calculated $\delta^{18}O_{IVF\text{-}SW}$ (blue circles with weighted 3-point smooth) from the Florida Straits (JPC26). **(B)** *N. dutertrei* abundances (purple circles with weighted 3-point smooth) in Florida Straits (JPC26). **(C)** Benthic $\delta^{18}O_{IVF\text{-}C}$ record (orange circles) in JPC26 [*Lynch-Stieglitz et al.*, in prep]. Note the response of benthic $\delta^{18}O_{IVF\text{-}C}$ values before planktic changes across H2.

APPENDIX B

Table 1. AMS ^{14}C and Calendar Ages

Core	Depth, cm	^{14}C Age	Error, yrs	Calendar age, ka B.P.	Reference
JPC26	848.25	20300	120	23.760	*Lynch-Stieglitz et al., 2011*
JPC26	878.25	21300	95	24.896	*This study*
JPC26	952.25	26300	130	30.693	*Lynch-Stieglitz et al., 2011*
JPC26	1014.25	28200	180	31.890	*Lynch-Stieglitz et al., 2011*
JPC26	1032.25	28200	590	32.160	*Lynch-Stieglitz et al., 2011*
JPC26	1074.25	29300	380	33.482	*Lynch-Stieglitz et al., 2011*
JPC26	1104.25	30600	170	34.800	*This study*
JPC26	1118.25	30900	220	34.958	*Lynch-Stieglitz et al., 2011*

APPENDIX C

JPC26 Geochemical Data

Depth (cm)	Probable Ages (Years BP)	Tuned Ages (Years BP)	$\delta^{18}O_C$	Mg/Ca (mmol/mol)	Ba/Ca (µmol/mol)	SST	$\delta^{18}O_{SW}$	$\delta^{18}O_{IVF-SW}$
784.25	20137	20007	0.4	3.21	0.88	23.69	2.16	1.13
786.25	20251	20112	0.61	3.18	0.92	23.61	2.35	1.32
788.25	20364	20218	0.8	3.19	0.94	23.65	2.55	1.51
790.25	20477	20323	0.43	3.40	0.97	24.33	2.32	1.28
792.25	20590	20428	0.69	2.81	0.95	22.21	2.14	1.10
794.25	20703	20533	0.38	3.02	1.20	23.02	2.00	0.95
796.25	20817	20638	0.91	3.25	0.97	23.85	2.70	1.65
798.25	20930	20743	0.97	3.08	1.05	23.27	2.64	1.59
800.25	21043	20848	0.51	3.38	1.04	24.27	2.39	1.34
802.25	21156	20953	0.54	3.14	1.03	23.46	2.25	1.20
804.25	21269	21058	0.88	3.32	0.96	24.08	2.72	1.66
806.25	21383	21163	0.67	3.33	1.04	24.12	2.52	1.46
808.25	21496	21268	0.47	3.13	1.00	23.41	2.17	1.11
810.25	21609	21373	0.4	3.26	1.04	23.88	2.20	1.14
812.25	21722	21479	0.31	3.43	1.09	24.45	2.23	1.17
814.25	21835	21584	0.66	3.17	1.00	23.56	2.39	1.33
816.25	21949	21689	0.41	3.44	1.10	24.49	2.33	1.28
818.25	22062	21794	0.8	3.25	1.14	23.86	2.59	1.54
820.25	22175	21899	0.44	3.28	0.96	23.95	2.25	1.20
822.25	22288	22004	0.69	3.13	1.08	23.43	2.39	1.34
824.25	22402	22109	0.44	3.39	1.13	24.32	2.33	1.28
826.25	22515	22214	0.65	3.23	1.15	23.78	2.43	1.38
828.25	22628	22319	0.67	3.09	1.18	23.30	2.35	1.30
830.25	22741	22424	0.56	3.69	1.07	25.25	2.64	1.60
832.25	22854	22529	0.11	3.52	1.14	24.74	2.09	1.05
834.25	22968	22634	0.11	3.74	1.02	25.42	2.23	1.19
836.25	23081	22740		3.94	0.98	25.98		
838.25	23194	22845	0.7	3.57	1.11	24.89	2.71	1.67
840.25	23307	22950	0.2	3.33	1.05	24.13	2.05	1.01
842.25	23420	23055	0.54	4.39	1.20	27.18	3.02	1.99
844.25	23534	23160	0.73	4.20	1.15	26.70	3.11	2.09
846.25	23647	23265	0.67	3.99	0.97	26.12	2.93	1.91
848.25	23760	23370	0	3.06	0.88	23.18	1.65	0.63

850.25	23836	23472	0.84	3.56	0.89	24.85	2.84	1.82
852.25	23911	23573	0.56	3.68	0.99	25.22	2.63	1.62
854.25	23987	23675	0.8	3.40	1.03	24.33	2.69	1.68
856.25	24063	23777	0.46	3.43	1.05	24.43	2.37	1.36
858.25	24139	23879	0.15	3.43	1.01	24.45	2.07	1.06
860.25	24214	23980	0.27	3.26	0.96	23.89	2.07	1.07
862.25	24290	24082	0.26	3.43	1.00	24.46	2.18	1.18
864.25	24366	24184	0.7	3.71	1.00	25.32	2.80	1.80
866.25	24442	24286	0.48	3.59	0.97	24.96	2.50	1.51
868.25	24517	24387	0.97	3.45	1.02	24.51	2.90	1.91
870.25	24593	24489	0.9	3.55		24.83	2.89	1.91
872.25	24669	24591	0.38	3.41	1.05	24.37	2.28	1.29
874.25	24745	24693	0.81	3.47	1.02	24.57	2.75	1.77
876.25	24820	24794	0.89	4.04	1.13	26.27	3.18	2.21
878.25	24896	24896	0.54	3.82	1.04	25.65	2.71	1.73
880.25	25053	25057						
882.25	25209	25218						
884.25	25366	25379						
886.25	25523	25540	0.2	3.59	1.01	24.96	2.22	1.28
888.25	25679	25701	0.18	3.36	0.83	24.21	2.05	1.11
890.25	25836	25862	0.66	3.62	1.06	25.03	2.70	1.76
892.25	25993	26022	0.25	3.45	1.04	24.51	2.18	1.25
894.25	26149	26183	0.63	3.67	0.97	25.19	2.70	1.78
896.25	26306	26344	0.17	3.54	0.94	24.78	2.16	1.24
898.25	26463	26505	0.48	4.02	0.93	26.20	2.76	1.85
900.25	26619	26666	0.41	3.54	1.11	24.79	2.40	1.50
902.25	26776	26827	0.55	3.28	1.05	23.93	2.36	1.46
904.25	26933	26988	0.22	3.22	0.87	23.74	1.99	1.10
906.25	27089	27149	0.56	3.43	0.82	24.45	2.48	1.60
908.25	27246	27310	0.7	3.32	0.91	24.08	2.54	1.66
910.25	27403	27471	0.23	3.46	0.89	24.53	2.16	1.29
912.25	27559	27632	-0.07	3.43	0.86	24.44	1.84	0.99
914.25	27716	27793	0.4	3.23	0.77	23.77	2.17	1.33
916.25	27873	27953	0.32	3.44	0.81	24.47	2.24	1.40
918.25	28030	28114	0.61	3.48	0.85	24.60	2.56	1.73
920.25	28186	28275	-0.07	3.58	1.13	24.92	1.94	1.13
922.25	28343	28436	0.46	3.42	0.99	24.41	2.37	1.56
924.25	28500	28597	0.09	4.14	1.02	26.54	2.44	1.64
926.25	28656	28758	0.23	3.48	0.86	24.61	2.18	1.39
928.25	28813	28919	0.56	3.67	0.93	25.21	2.63	1.86

930.25	28970	29080	0.51	3.40	0.84	24.34	2.40	1.64
932.25	29126	29241	0.42	3.80	0.90	25.58	2.57	1.81
934.25	29283	29402	0.6	3.44	0.89	24.48	2.52	1.76
936.25	29440	29563	0.28	3.80	1.02	25.59	2.43	1.68
938.25	29596	29724	0.44	3.38	0.77	24.28	2.32	1.58
940.25	29753	29884	0.54	3.47	0.83	24.59	2.48	1.75
942.25	29910	30045	0.33	3.66	0.87	25.17	2.40	1.66
944.25	30066	30206		3.55	0.93	24.83		
946.25	30223	30367	0.61	3.63	0.99	25.07	2.65	1.93
948.25	30380	30528	0.23	3.80	1.11	25.59	2.38	1.66
950.25	30536	30689	0.38	3.94	0.91	25.99	2.62	1.90
952.25	30693	30850	0.26	3.52	0.84	24.74	2.24	1.53
954.25	30732	30881	0.14	4.20	0.84	26.69	2.52	1.81
956.25	30770	30911	0.19	3.90	0.93	25.87	2.40	1.69
958.25	30809	30942	0.49	3.61	0.91	25.03	2.53	1.82
960.25	30847	30973	0.07	3.48	0.98	24.62	2.02	1.31
962.25	30886	31003	0.455	3.80	0.82	25.58	2.60	1.90
964.25	30925	31034	0.56	3.92	0.93	25.93	2.78	2.08
966.25	30963	31065	0.41	3.69	0.89	25.25	2.49	1.79
968.25	31002	31095	0.28	3.67	0.79	25.19	2.35	1.65
970.25	31041	31126	0.325	3.74	0.78	25.41	2.44	1.74
972.25	31079	31156	0.1	3.65	0.81	25.13	2.16	1.45
974.25	31118	31187	0.66	3.39	0.79	24.31	2.55	1.84
976.25	31156	31218	0.06	3.69	0.74	25.26	2.14	1.44
978.25	31195	31248	0.38	3.98	0.88	26.11	2.64	1.94
980.25	31234	31279		4.09	0.76	26.40		
982.25	31272	31310	0.18	3.58	0.82	24.92	2.19	1.49
984.25	31311	31340	0.16	3.49	0.75	24.63	2.11	1.41
986.25	31349	31371	0.04	3.56	0.73	24.86	2.04	1.34
988.25	31388	31402	0.41	3.51	0.78	24.69	2.38	1.68
990.25	31427	31432	0.54	3.66	0.73	25.16	2.60	1.91
992.25	31465	31463	0.07	3.79	0.79	25.55	2.21	1.52
994.25	31504	31494	0.05	3.65	0.82	25.13	2.11	1.41
996.25	31542	31524	0.41	3.77	0.93	25.48	2.54	1.85
998.25	31581	31555	0.23	3.86	0.75	25.76	2.42	1.72
1000.25	31620	31585	0.13	4.06	0.78	26.31	2.43	1.74
1002.25	31658	31616	0.12	3.44	0.75	24.49	2.04	1.35
1004.25	31697	31647	-0.07	3.76	0.77	25.46	2.06	1.37
1006.25	31736	31677	0.15	3.31	0.76	24.05	1.98	1.29
1008.25	31774	31708	0.13	3.56	0.77	24.85	2.13	1.44

1010.25	31813	31739	0.37	3.59	0.82	24.94	2.39	1.70
1012.25	31851	31769	0.06	3.51	0.79	24.71	2.03	1.34
1014.25	31890	31800	-0.29	3.38	0.79	24.29	1.59	0.91
1016.25	31936	31827	0.04	3.37	0.73	24.27	1.92	1.23
1018.25	31981	31853	0.25	3.33	0.75	24.10	2.09	1.41
1020.25	32027	31880	0.34	3.73	0.89	25.37	2.45	1.76
1022.25	32072	31907	0.4	3.12	0.62	23.41	2.10	1.41
1024.25	32118	31933	0	3.46	0.81	24.56	1.94	1.25
1026.25	32163	31960	0.39	3.29	0.72	24.00	2.21	1.53
1028.25	32209	31987	0.23	3.63	0.71	25.09	2.28	1.60
1030.25	32254	32013	-0.03	3.56	0.75	24.86	1.97	1.29
1032.25	32300	32040	-0.04					
1034.25	32356	32067	-0.1	3.51	0.73	24.69	1.87	1.18
1036.25	32413	32093	-0.11	3.73	0.89	25.37	2.00	1.31
1038.25	32469	32120	-0.04	3.44	0.80	24.48	1.88	1.20
1040.25	32525	32147	-0.22	3.77	0.78	25.50	1.91	1.23
1042.25	32581	32173	-0.41	3.63	0.76	25.06	1.63	0.95
1044.25	32638	32200	-0.5	4.00	0.79	26.16	1.77	1.09
1046.25	32694	32227	-0.38	4.10	0.88	26.43	1.95	1.26
1048.25	32750	32253	-0.35	3.74	0.82	25.40	1.76	1.08
1050.25	32807	32280	-0.37	3.74	0.77	25.42	1.75	1.06
1052.25	32863	32307		4.07	0.87	26.34		
1054.25	32919	32333	-0.39	3.53	0.89	24.75	1.59	0.90
1056.25	32975	32360	-0.34	3.35	0.73	24.19	1.52	0.84
1058.25	33032	32387	-0.07	3.93	0.80	25.95	2.16	1.47
1060.25	33088	32413	0.1	3.92	0.82	25.93	2.32	1.64
1062.25	33144	32440	-0.53	3.59	0.76	24.95	1.49	0.80
1064.25	33201	32467	-0.31	3.33	0.69	24.10	1.53	0.85
1066.25	33257	32493	0.29	4.10	0.84	26.43	2.62	1.93
1068.25	33313	32520	0.18	3.34	0.77	24.14	2.03	1.35
1070.25	33369	32547	0.53	3.54	0.78	24.80	2.52	1.83
1072.25	33426	32573	0.01	3.50	0.73	24.67	1.97	1.28
1074.25	33482	32600	0.01	3.77	0.77	25.51	2.15	1.46
1076.25	33570	32747	0.05	3.60	0.71	24.99	2.08	1.39
1078.25	33658	32893	0.22	3.80	0.77	25.57	2.37	1.68
1080.25	33746	33040	-0.17	3.81	0.73	25.62	1.99	1.30
1082.25	33833	33187	0.45	3.69	0.74	25.27	2.54	1.85
1084.25	33921	33333	0.42	3.56	0.64	24.85	2.42	1.73
1086.25	34009	33480	-0.21	3.25	0.77	23.84	1.58	0.89
1088.25	34097	33627	-0.05	3.31	0.78	24.05	1.78	1.09

1090.25	34185	33773	0.01	3.66	0.77	25.17	2.07	1.38
1092.25	34273	33920	-0.09	3.51	0.67	24.72	1.88	1.18
1094.25	34361	34067	-0.27	4.02	0.70	26.21	2.01	1.31
1096.25	34449	34213	-0.09	3.24	0.84	23.81	1.69	0.99
1098.25	34536	34360	0.15	3.40	0.70	24.36	2.05	1.34
1100.25	34624	34507	-0.04	3.67	0.74	25.19	2.03	1.33
1102.25	34712	34653	-0.4	3.19	0.72	23.62	1.34	0.64
1104.25	34800	34800	-0.19	3.22	0.72	23.76	1.58	0.88
1106.25	34823	34882	-0.3	3.54	0.70	24.79	1.69	0.98
1108.25	34845	34963	0.17	3.73	0.71	25.39	2.28	1.57
1110.25	34868	35045	-0.01	3.45	0.59	24.50	1.92	1.21
1112.25	34890	35127	-0.45	3.72	0.63	25.34	1.65	0.94
1114.25	34913	35209	0.17	3.77	0.81	25.50	2.30	1.60
1116.25	34935	35290		3.92	0.90	25.94		
1118.25	34958	35372	-0.04	3.87	0.78	25.80	2.16	1.45
1120.25	34981	35454	-0.29	4.07	0.72	26.35	2.02	1.32

APPENDIX D

JPC26 Foraminiferal Abundance Data

Depth (cm)	Probable Ages (Years BP)	Tuned Ages (Years BP)	*N. dutertrei* per gram
784.25	20137	20007	10.7
786.25	20251	20112	6.9
788.25	20364	20218	5.5
790.25	20477	20323	4.7
792.25	20590	20428	6.0
794.25	20703	20533	9.6
796.25	20817	20638	2.4
798.25	20930	20743	1.9
800.25	21043	20848	1.4
802.25	21156	20953	2.8
804.25	21269	21058	10.4
806.25	21383	21163	7.4
808.25	21496	21268	11.0
810.25	21609	21373	3.6
812.25	21722	21479	7.2
814.25	21835	21584	6.3
816.25	21949	21689	7.4
818.25	22062	21794	7.0
820.25	22175	21899	6.8
822.25	22288	22004	10.5
824.25	22402	22109	5.0
826.25	22515	22214	9.8
828.25	22628	22319	9.1
830.25	22741	22424	9.2
832.25	22854	22529	10.9
834.25	22968	22634	15.9
836.25	23081	22740	12.9
838.25	23194	22845	11.3
840.25	23307	22950	6.3
842.25	23420	23055	15.0
844.25	23534	23160	8.7
846.25	23647	23265	5.4
848.25	23760	23370	10.5

850.25	23836	23472	19.9
852.25	23911	23573	6.1
854.25	23987	23675	12.0
856.25	24063	23777	12.1
858.25	24139	23879	12.6
860.25	24214	23980	26.3
862.25	24290	24082	16.4
864.25	24366	24184	3.0
866.25	24442	24286	0.0
868.25	24517	24387	9.3
870.25	24593	24489	6.5
872.25	24669	24591	9.8
874.25	24745	24693	7.2
876.25	24820	24794	6.0
878.25	24896	24896	3.5
880.25	25053	25057	
882.25	25209	25218	
884.25	25366	25379	
886.25	25523	25540	11.6
888.25	25679	25701	8.2
890.25	25836	25862	7.2
892.25	25993	26022	0.0
894.25	26149	26183	6.9
896.25	26306	26344	12.8
898.25	26463	26505	18.3
900.25	26619	26666	14.7
902.25	26776	26827	8.9
904.25	26933	26988	5.0
906.25	27089	27149	10.2
908.25	27246	27310	9.3
910.25	27403	27471	5.5
912.25	27559	27632	13.5
914.25	27716	27793	14.5
916.25	27873	27953	8.7
918.25	28030	28114	9.2
920.25	28186	28275	15.2
922.25	28343	28436	23.1
924.25	28500	28597	24.2

926.25	28656	28758	18.2
928.25	28813	28919	18.4
930.25	28970	29080	7.6
932.25	29126	29241	13.1
934.25	29283	29402	7.5
936.25	29440	29563	9.5
938.25	29596	29724	5.4
940.25	29753	29884	3.5
942.25	29910	30045	8.4
944.25	30066	30206	9.7
946.25	30223	30367	3.4
948.25	30380	30528	8.9
950.25	30536	30689	10.7
952.25	30693	30850	7.0
954.25	30732	30881	10.8
956.25	30770	30911	3.5
958.25	30809	30942	7.7
960.25	30847	30973	9.8
962.25	30886	31003	7.2
964.25	30925	31034	13.3
966.25	30963	31065	22.7
968.25	31002	31095	19.0
970.25	31041	31126	5.0
972.25	31079	31156	24.0
974.25	31118	31187	25.6
976.25	31156	31218	11.3
978.25	31195	31248	9.4
980.25	31234	31279	22.5
982.25	31272	31310	13.4
984.25	31311	31340	8.8
986.25	31349	31371	16.2
988.25	31388	31402	14.7
990.25	31427	31432	29.8
992.25	31465	31463	23.4
994.25	31504	31494	26.5
996.25	31542	31524	33.5
998.25	31581	31555	21.7
1000.25	31620	31585	13.4

1002.25	31658	31616	23.4
1004.25	31697	31647	28.7
1006.25	31736	31677	19.6
1008.25	31774	31708	22.7
1010.25	31813	31739	23.2
1012.25	31851	31769	15.8
1014.25	31890	31800	49.5
1016.25	31936	31827	31.2
1018.25	31981	31853	7.9
1020.25	32027	31880	15.0
1022.25	32072	31907	1.9
1024.25	32118	31933	13.9
1026.25	32163	31960	20.6
1028.25	32209	31987	3.5
1030.25	32254	32013	28.4
1032.25	32300	32040	13.6
1034.25	32356	32067	12.1
1036.25	32413	32093	20.4
1038.25	32469	32120	32.7
1040.25	32525	32147	31.4
1042.25	32581	32173	44.3
1044.25	32638	32200	26.5
1046.25	32694	32227	12.7
1048.25	32750	32253	23.8
1050.25	32807	32280	38.1
1052.25	32863	32307	21.2
1054.25	32919	32333	35.1
1056.25	32975	32360	17.3
1058.25	33032	32387	33.5
1060.25	33088	32413	36.1
1062.25	33144	32440	19.8
1064.25	33201	32467	19.0
1066.25	33257	32493	19.4
1068.25	33313	32520	8.8
1070.25	33369	32547	11.0
1072.25	33426	32573	0.0
1074.25	33482	32600	7.5
1076.25	33570	32747	0.0

1078.25	33658	32893	0.0
1080.25	33746	33040	3.0
1082.25	33833	33187	10.3
1084.25	33921	33333	16.9
1086.25	34009	33480	30.7
1088.25	34097	33627	42.3
1090.25	34185	33773	17.8
1092.25	34273	33920	14.4
1094.25	34361	34067	16.0
1096.25	34449	34213	18.5
1098.25	34536	34360	23.6
1100.25	34624	34507	27.8
1102.25	34712	34653	31.3
1104.25	34800	34800	28.0
1106.25	34823	34882	24.8
1108.25	34845	34963	12.1
1110.25	34868	35045	22.7
1112.25	34890	35127	18.0
1114.25	34913	35209	56.0
1116.25	34935	35290	33.7
1118.25	34958	35372	12.0
1120.25	34981	35454	25.9

VITA

Theodore Roland Them, II received his Bachelor of Science degree in Geoenvironmental Studies from Shippensburg University of Pennsylvania in 2008. He entered the Oceanography program at Texas A&M University in January 2010 and will receive his Master of Science degree in August 2012. He will subsequently begin his studies toward the Doctor of Philosophy degree at Virginia Polytechnic and State University. His research interests include sedimentary geochemistry, micropaleontology, paleoceanography, and paleoclimatology.

Mr. Them may be reached at 407 Piedmont St., Blacksburg, VA 24060. His email is teddythem@gmail.com.